WL-TR-94-7100

HARDENING AND REHABILITATION OF CONCRETE STRUCTURES USING CARBON FIBER REINFORCED PLASTICS (CFRP)

Dr. C. Allen Ross

University of Florida
Graduate Engineering and Research Center
P O Box 1918
Eglin AFB FL 32542-0918

David M. Jerome

Wright Laboratory Armament Directorate
Assessment and Instrumentation Division
Technology Assessment Branch
Eglin AFB FL 32542-6810

M. L. Hughes

Wright Laboratory Flight Dynamics Directorate
Vehicle Subsystems Division
Air Base Technology Branch
Tyndall AFB FL 32403-5323

December 1994

FINAL REPORT FOR PERIOD APRIL 1994 - SEPTEMBER 1994

WRIGHT LABORATORY ARMAMENT DIRECTORATE
Air Force Materiel Command ▮ United States Air Force ▮ Eglin Air Force Base

NOTICE

When Government drawings, specifications, or other data are used for any purpose other than in connection with a definitely Government-related procurement, the United States Government incurs no responsibility or any obligation whatsoever. The fact that the Government may have formulated or in any way supplied the said drawings, specifications, or other data, is not to be regarded by implication, or otherwise as in any manner construed, as licensing the holder, or any other person or corporation; or as conveying any rights or permission to manufacture, use, or sell any patented invention that may in any way be related thereto.

This technical report has been reviewed and is approved for publication.

FOR THE COMMANDER

WALTER O. MAINE
Chief, Assessment and Instrumentation Division

If your address has changed, if you wish to be removed from our mailing list, or if your organization no longer employs the addressee, please notify WL/MNSA, Eglin AFB FL 32542-6810, to help us maintain a current mailing list.

Do not return copies of this report unless contractual obligations or notice on a specific document requires that it be returned.

REPORT DOCUMENTATION PAGE

Form Approved
OMB No. 0704-0188

1. AGENCY USE ONLY (Leave blank)	2. REPORT DATE	3. REPORT TYPE AND DATES COVERED
	December 1994	Final, 19 Apr 94 - 30 Sep 94

4. TITLE AND SUBTITLE Hardening and Rehabilitation of Concrete Structures Using Carbon Fiber Reinforced Plastics (CFRP)

5. FUNDING NUMBERS
C: FO8635-92-C-0032
PE: 62602F
PR: 2543
TA: 94-02
WU:

6. AUTHOR(S)
C. Allen Ross
David M. Jerome, M. L. Hughes

7. PERFORMING ORGANIZATION NAME(S) AND ADDRESS(ES)
University of Florida
Graduate Engineering Research Center
P O BOX 1918
Eglin AFB, FL 32542-0918

8. PERFORMING ORGANIZATION REPORT NUMBER

9. SPONSORING / MONITORING AGENCY NAME(S) AND ADDRESS(ES)
Wright Laboratory Armament Directorate
Technology Assessment Branch (WL/MNSA)
101 West Eglin Blvd., Suite 326
Eglin AFB, FL 32542-6810

10. SPONSORING / MONITORING AGENCY REPORT NUMBER
WL-TR-94-7100

11. SUPPLEMENTARY NOTES

12a. DISTRIBUTION / AVAILABILITY STATEMENT
Approved for Public Release;
Distribution Unlimited

12b. DISTRIBUTION CODE
A

13. ABSTRACT *(Maximum 200 words)*

Carbon Fiber Reinforced Plastic (CFRP) panels were externally bonded to conventionally reinforced steel concrete beams. The CFRP beams were statically tested to their maximum load in a third-point loading device. Elastic-plastic section analyses and a numerical Finite Element Method (FEM) analysis were performed on the beams. Good agreement between the section analysis and the experiment was obtained. Considerable strength enhancement was obtained when the CFRP was added to the bottom of concrete beams with tensile steel reinforcement of less than one percent. For beams with less than one percent steel and CFRP, the failure was by delamination between the CFRP and the adhesive. Improvements in bond strength between the CFRP and adhesive is needed to increase the strength enhancement.

14. SUBJECT TERMS	15. NUMBER OF PAGES
Carbon Fiber, Composites, Structural Rehabilitation, Concrete Strengthening, Section Analysis	50
	16. PRICE CODE

17. SECURITY CLASSIFICATION OF REPORT	18. SECURITY CLASSIFICATION OF THIS PAGE	19. SECURITY CLASSIFICATION OF ABSTRACT	20. LIMITATION OF ABSTRACT
Unclassified	Unclassified	Unclassified	SAR

List of Figures

List of Figures

Section I

INTRODUCTION

1. Objective

The major objective of this study was to observe static tests of conventional concrete beams fitted with bottom carbon fiber reinforced plastic (CFRP) panels and develop analyses of such beams for prediction of load-displacement response.

2. Background

Fiber Reinforced Plastics (FRP) have been used extensively, ranging from high performance aerospace applications to the mundane patching of holes in automobiles and boats. The literature is full of applications of fibrous material and recently, several complete pedestrian bridges have been fabricated using FRP. A recent application of Carbon Fiber Reinforced Plastics (CFRP) to strengthening of a conventionally reinforced concrete bridge in Switzerland is described by Meier et al. [1]. In a specific case, a 6.2 kg panel of CFRP was used instead of 175 kg steel plate to repair a concrete box beam of a bridge. The CFRP sheets were 2mm thick, 150mm wide and 5m long. Meier [2] also presented a feasibility study on the use of CFRP in other rehabilitation applications where steel repair plates may be replaced with the advanced composite panels. It appears that Kaiser [3] first employed CFRP for strengthening of concrete beams as early as 1989. Triantafillou et al. [4] describes the use of CFRP panels as prestressing for laboratory size steel reinforced concrete beams.

In the above references the CFRP panels were all applied to the tension side of the beams as shown in Figure 1. The major advantage of these applications is that a very thin (approximately 0.5 - 1.00mm or 0.02 - 0.04 inch) lightweight carbon/epoxy laminate is cemented to the tension side of the beam. Using an unidirectional fiber laminate, with the fibers running parallel to the longitudinal axis of the beam, places the fibers in their best position and direction to take advantage of their high tensile strength (1.03 - 2.07 GPa, 150,000 - 300,000 psi).

The use of the CFRP on only the tension side of a concrete beam has been shown to considerably improve its load carrying capacity. Some recent (1993) concrete/CFRP work has been accomplished at Wright Laboratory (WL/FIVC), Tyndall AFB, under the direction of Dr. R. L. Sierakowski, Ohio State University, Dr. J. W. Tedesco, Auburn University, and Dr. C. A. Ross, University of Florida.

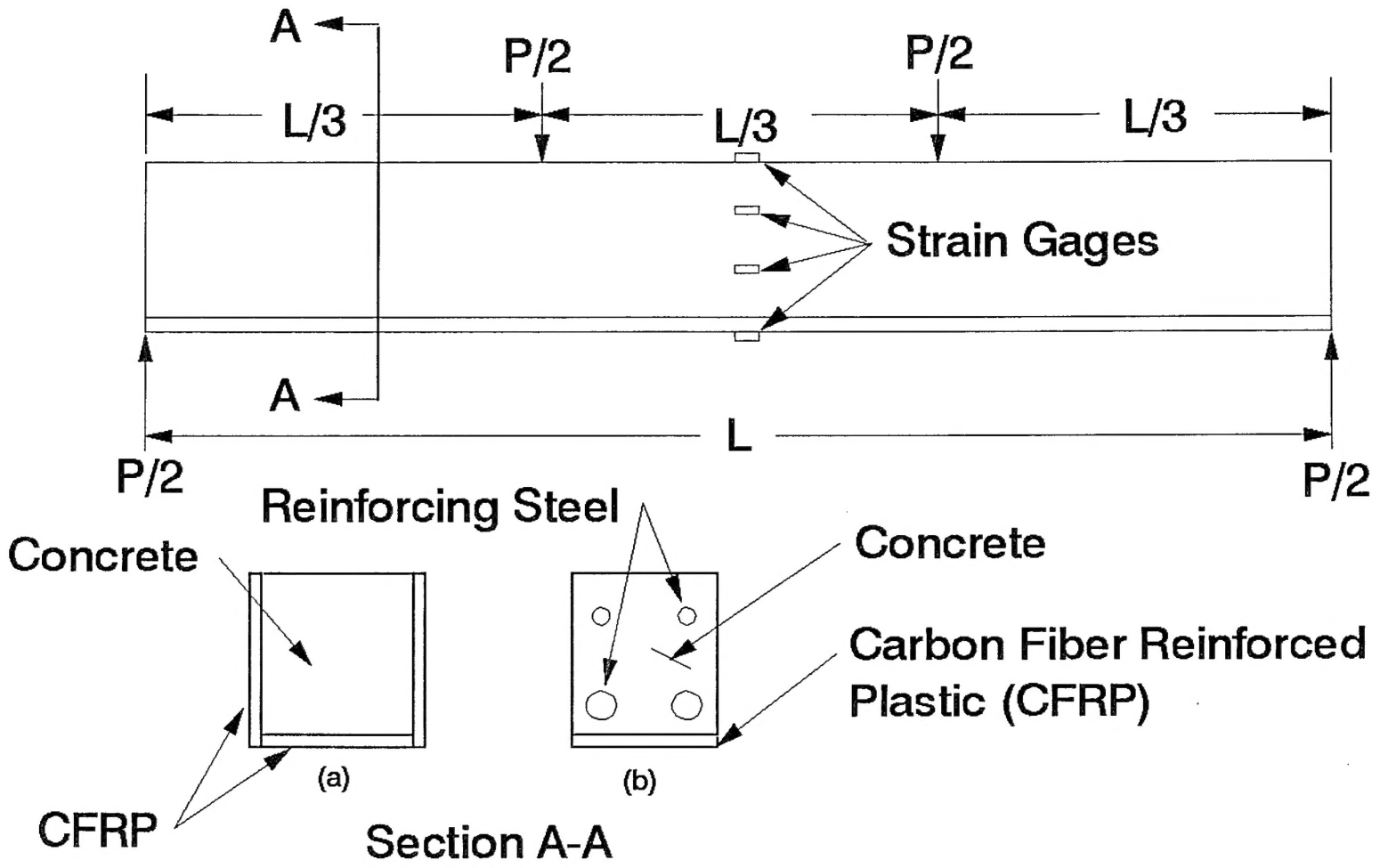

TYPES OF BEAMS TESTED

1. Plain concrete
2. Plain concrete with bottom CFRP
3. Plain concrete with bottom and side CFRP
4. R/C beams
5. R/C with bottom CFRP
6. R/C with bottom and side CFRP

Figure 1. Tension Reinforcement of Concrete Beams Using CFRP.

Small laboratory size plain concrete beams of 25x25x305mm, 51x51x305mm, and 76x76x760mm (1 x 1 x 12 in; 2 x 2 x 12 in, and 3 x 3 x 30 in) with CFRP laminates cemented on both bottom (tension) and sides have been tested statically. Results show that the proper placement of the CFRP laminates improved the bending load capacities as much as 5 to 8 times that of a plain concrete beam. The most important result of these laboratory tests was that placing the CFRP laminate along the sides of the beams (Figure 1b) was very effective in preventing low load shear and diagonal tension failures of the beams. Results of the above work are discussed in Reference 5. These results may prove very useful in an effort to rehabilitate beams showing multiple cracking from distress of overloading or deterioration of steel reinforcement. Since the publications by Meier [1,2] and Kaiser [3], a considerable number of publications have appeared and several are listed as References 6 to 8.

3. Scope/Approach

The general approach in this study was, (1) to build twenty-four concrete beams with varying steel reinforcement ratios, apply a three ply CFRP to each beam on bottom only, test each beam to its maximum load while recording load, displacement and strain and 2) using elastic/plastic section analysis and numerical analysis, derive relations for predicting load-displacement response of conventionally steel reinforced concrete beams with external CFRP panels.

The beams were to be fabricated and tested by WL/FIVCS of Tyndall AFB and beam analysis was to be performed by Dr. C. Allen Ross of University of Florida Graduate Engineering Research Center (UFGERC).

Section II

EXPERIMENTAL TESTS

1. Test Apparatus and Equipment

   a. Main Test Frame

The main test frame was designed and built by WL/FIVCS at Tyndall AFB, FL. This main test frame is capable of producing a total load of 100 kilopounds (kips) (444.8kn) in a third-point loading mode. (A third-point loading is a special case of four point loading where the beam is divided into L/3 pieces as shown in Figure 1.) See Figure 2 for a photograph and Figure 3 for a schematic of the main test frame. The device is limited to beams 10 feet (3.05m) in length with a load span of 9 feet (2.95m). The four loading points are seperated by 3 feet (0.9m) and the load readings are given as the sum of the two center loading rams. The ram load is applied by a hand controlled hydraulic pump. Loading rates varied but on the average were approximately 5lb/sec (22.25N/sec).

   b. Instrumentation

Each test beam with CFRP attached was instrumented with four electrical resistance strain gages. (All strain gauges were obtained from Micromeasurements Inc®, Raleigh, NC.) Three strain gauges of 4.0in gauge length were mounted on top and sides of the CFRP beams (see Figure 8) and were placed on bare concrete. These strain gauges were of the type EA-06-40CBY-120 and were cemented with 24 hour epoxy cement. The concrete surface was filled with epoxy cement and sanded smooth before gauge installation. Strain gauges of 0.25 in (6.4 mm) gauge length (ED-DY-500BH-500) were cemented to the CFRP on the bottom of the beam. These gauges were also attached with 24 hour epoxy cement. Ectron® Model 563F strain gauge conditioners were used in the strain gauge data acquisition.

Linear Voltage Displacement Transducers (LVDT) of RDP-Electrosense® Type ACT 200C were used to measure midpoint beam displacement and relative displacement of a rotation cage mounted on the beam midspan position (see Figures 2 and 10).

All conditioned strain data and the LVDT data were fed to a data acquisition system consisting of a Halikar® 3865x Laptop Computer, a National Instrument® PC-LPM-16 data acquisition card

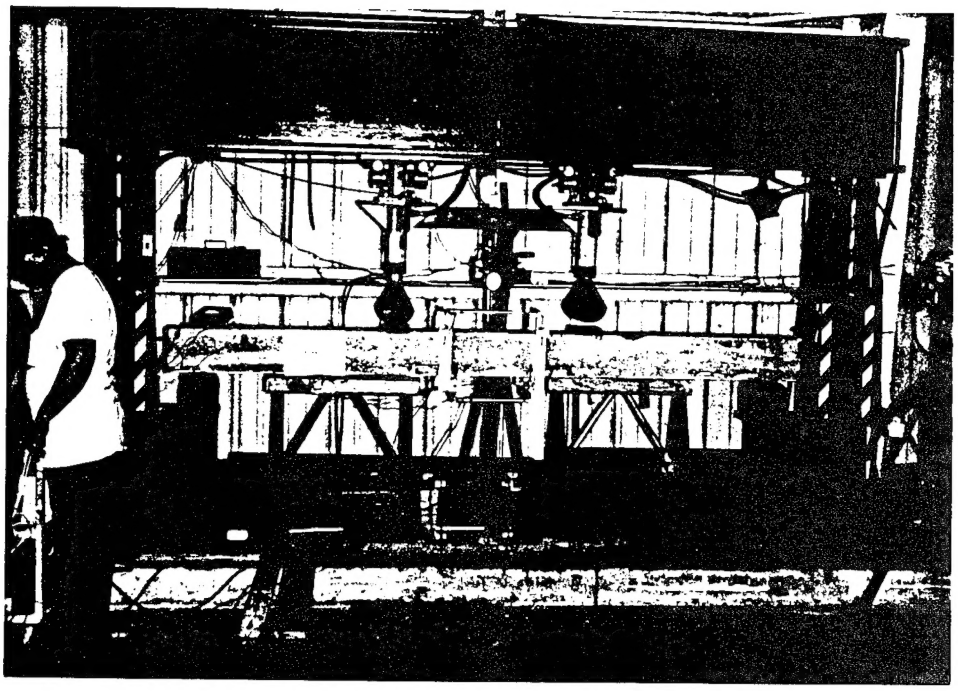

Figure 2. Photograph of WL/FIVCS test frame.

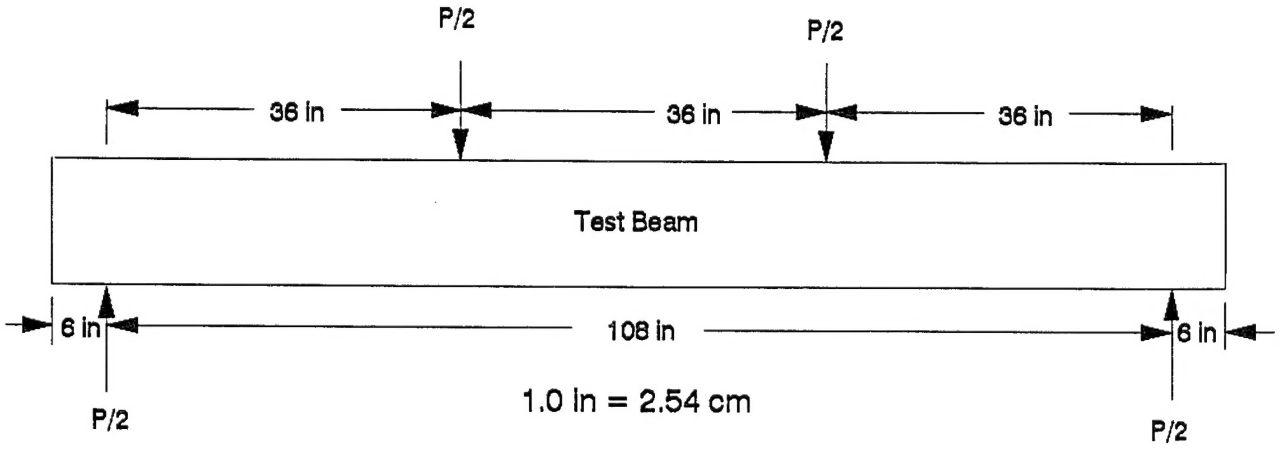

Figure 3. Schematic of WL/FIVCS test frame.

and a DAQWARE® software package. The data was then transferred to an ASCII file disk and processed in final form using a Lotus® 123 software package.

In addition, a large dial gauge was used to measure beam displacement. In all beam tests this dial gauge and the load indicator were monitored using a video camera.

2. Test Beam

a. Beam Fabrication

Concrete beams were cast in 8in x 8in x 10 ft (0.2m x 0.2m x 3.05m) steel molds using 7.95 ksi (54.8 MPa) strength concrete. The beams were conventionally reinforced with steel of 60 ksi (0.41 GPa) yield stress. Six different steel rod diameters were used for tensile reinforcement. A schematic of the steel placement and reinforcing rod sizes is given in Figure 4. No. 3 compression steel was used in all beams and the main purpose of this steel was to support the shear stirrups. A constant moment section free of shear stirrups was cast in the middle of each beam.

For each tensile steel size, three beams had CFRP attached and one beam without CFRP was tested as a control beam. The CFRP was obtained from WL/MLBC, Wright Patterson AFB in panels of size 108in x 8.0in x 0.0175in (2.74m x 0.203m x 0.45mm). The material classification for the CFRP is an AS4/1919 graphite/epoxy composite which is 60 percent graphite fiber by volume with a room temperature 0° tensile strength of 320 ksi (2.413 GPa) and a 0° tensile modulus of 20 Msi (138 GPa).

b. CFRP Placement

A three ply uniaxial panel of CFRP was attached to the tension side (bottom) of three beams for each steel reinforcement. Before the placement of the CFRP each concrete beam was wire brushed and cleaned with acetone. For No. 7 series beams the CFRP was cleaned with acetone. In all beams except 5D and 8B a Sikadur® 32 adhesive was used for cementing the CFRP to the concrete. For beams 5D and 8B a different adhesive, Dexter Hysol®, was used. In the case of 8B the peak load was approximately 10 percent higher than the 8C and 8D beams but beam 5B showed no strength increase over beams 5C and 5D.

After the adhesive was applied to the beams it was spread and smoothed by a saw tooth trowel. The CFRP was then placed atop the adhesive coated beam and a long flat steel channel was placed

Ten. Steel Table

Beam Series No.	Ten. Steel No. *
3A,B,C,D**	3
4A,B,C,D	4
5A,B,C,D	5
6A,B,C,D	6
7A,B,C,D	7
8A,B,C,D	8

*Nominal Rod Diameter
In 1/8s Of An Inch

**All Suffix A Beams
Tested Without CFRP

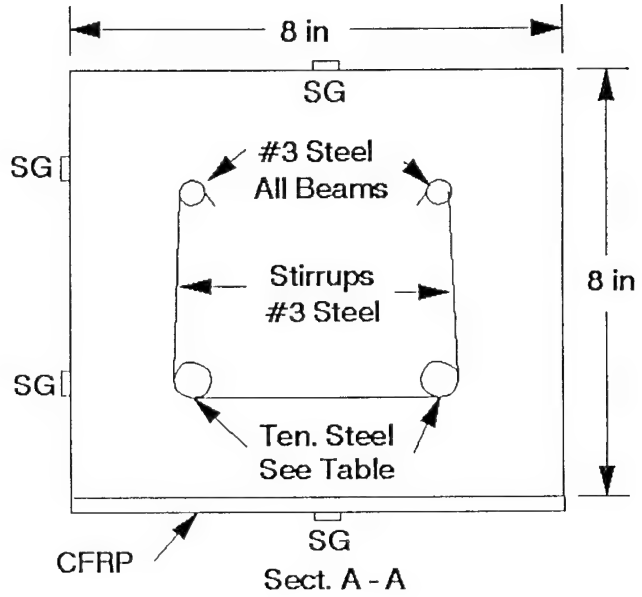

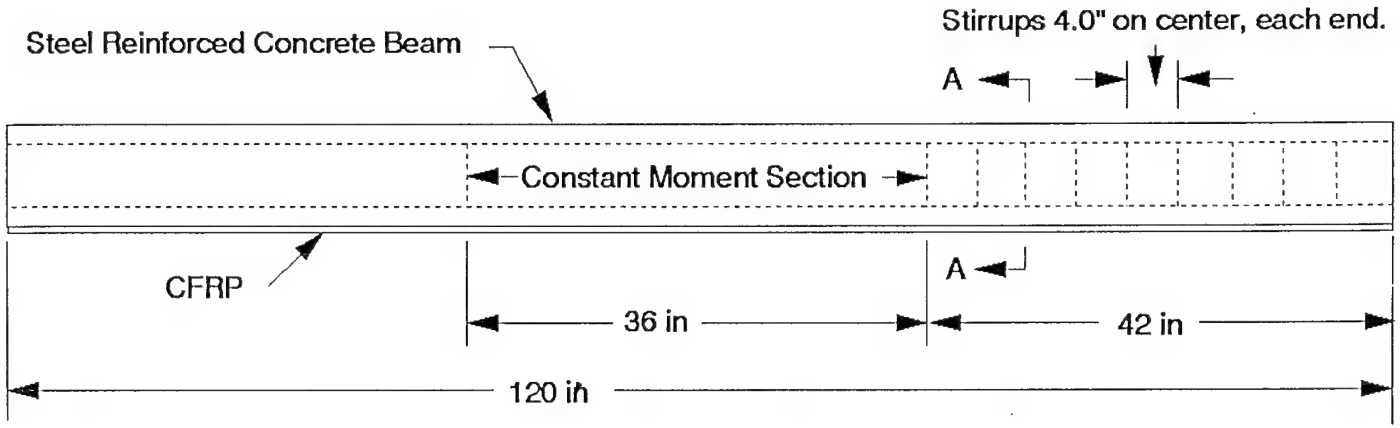

Figure 4. Schematic of test beams used in 1994 tests.

atop the CFRP. The steel channel was then loaded uniformly with a total of 500 lbs (2.224 kn). The adhesive was allowed to cure for approximately seven days.

3. Test Results

All test data and related dimensions were recorded using the English system of units. The data in this report are reported in the English system with proper notation for determining the data in SI units.

In the 1993 tests several kinds of beams were tested. These beams were nominally 8in x 8in x 120in (0.2m x 0.2m x 3.05m) and were tested in the same fashion as the 1994 tests. The results of the 1993 tests are shown in Figure 5 along with the concrete/steel/CFRP arrangement for each beam.

The peak experimental loads for the 1994 tests are shown in Table 1 along with notes indicating special treatment or remarks specific to certain tests.

In an effort to show the effects of the addition of the CFRP, an enhancement ratio, defined as the peak load for a given steel and CFRP beam divided by the peak load of a beam with only the same steel reinforcement, is displayed in Figure 6. This figure shows considerable enhancement for the addition of CFRP to the lower tensile steel ratios. However, the addition of CFRP to the higher tensile steel ratios shows very little enhancement.

Strain gages were placed on the beams at top and bottom and on sides as shown in Figure 8. In most all cases the strain measurements showed erratic readings indicating malfunctions in the strain conditioners. All strain conditioners used showed good initial balance and proper shunt calibration but gave erratic readings during the tests. Some tests gave reasonable results and the strain gage readings for beam 5B are shown in Figure 7. Figure 8 shows the distribution of strain at the peak load along with the gauge positions in the cross section. For this beam the strain distribution does not show exact linearity as was found in tests on smaller beams and several of the 1993 beam tests.

It was shown experimentally that there were generally two types of beam failures. For beams with the lower tensile steel rod sizes of Nos. 3, 4, and 5 the failure was delamination between the CFRP and the adhesive. For the higher tensile steel rod sizes of Nos. 6, 7, and 8 the failure was by crushing of the upper compression concrete accompanied by horizontal cracking at about the height

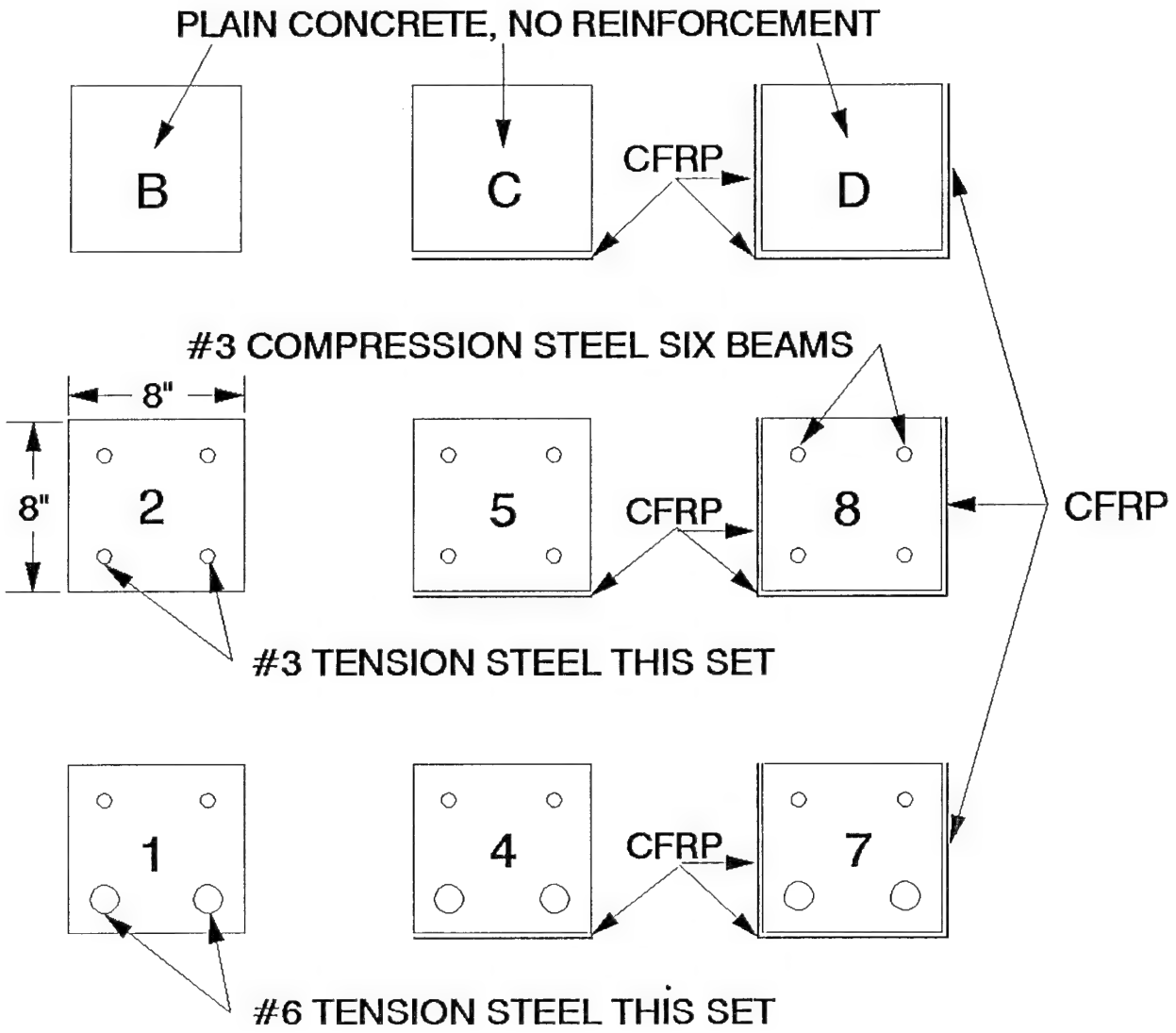

PEAK BENDING LOAD BEAM	LOAD kips(kN)
B	2.5(11.12)
C	6.2(27.58)
D	17.0(75.62)
2	6.0(26.69)
5	12.2(54.27)
8	18.53(82.42)
1	23.0(102.3)
4	31.0(137.89)
7	32.0(142.34)

Figure 5. Beam cross section configuration and peak experimental load for 1993 beam tests.

Table 1

Static Tests of CFRP Beams

(Summer 1994)

Beam*	Percent Steel	Peak Load klbs	Enhancement Ratio**	Apparent Failure Mode++
3A	0.46	6.0	N/A	N/A
3B		18.0	3.00	D
3C		16.0	2.67	D
4A	0.83	10.5	N/A	N/A
4B		22.0	2.10	D
4C		16.0	1.52	D
4D		18.0	1.71	D
5A	1.29	14.0(estimate)	N/A	N/A
5B		24.5	1.75	D
5C		24.3	1.74	D
5D		24.4***	1.75	D
6A+	1.83	16.0	N/A	N/A
6B+		24.2	1.51	C
6C+		23.5	1.47	C
6D+		25.0	1.56	C
7A	2.50	26.0	N/A	N/A
7B		33.0	1.27	C
7C		33.0	1.27	C
7D		32.7	1.26	C
8A	3.29	30.0	N/A	N/A
8B		38.0***	1.27	C
8C		34.4	1.15	C
8D		34.4	1.15	C

** Peak load CFRP beam/peak load control A beam, N/A denotes not applicable

*** Dexter Hysol adhesive, all others Sikadur adhesive

* Digit indicates tensile steel size.

Letter A indicates control beam with no CFRP.

Other letters denote CFRP.

+ Peak load lower than 1993 tests. Possible oil contamination from mold release agent.

++ D denotes delamination, C denotes compression upper surface.

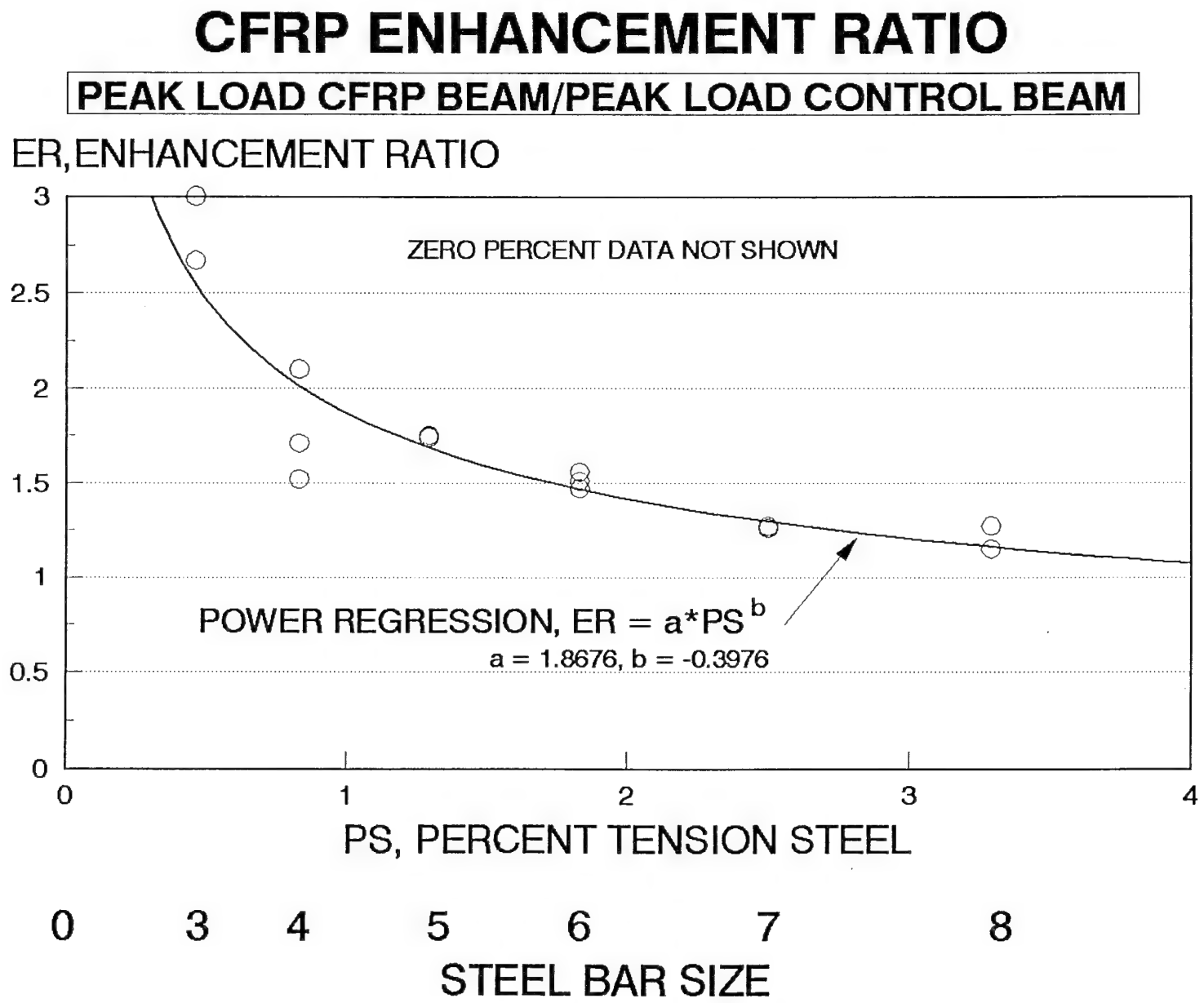

Figure 6. Enhancement ratios for 1994 beam tests.

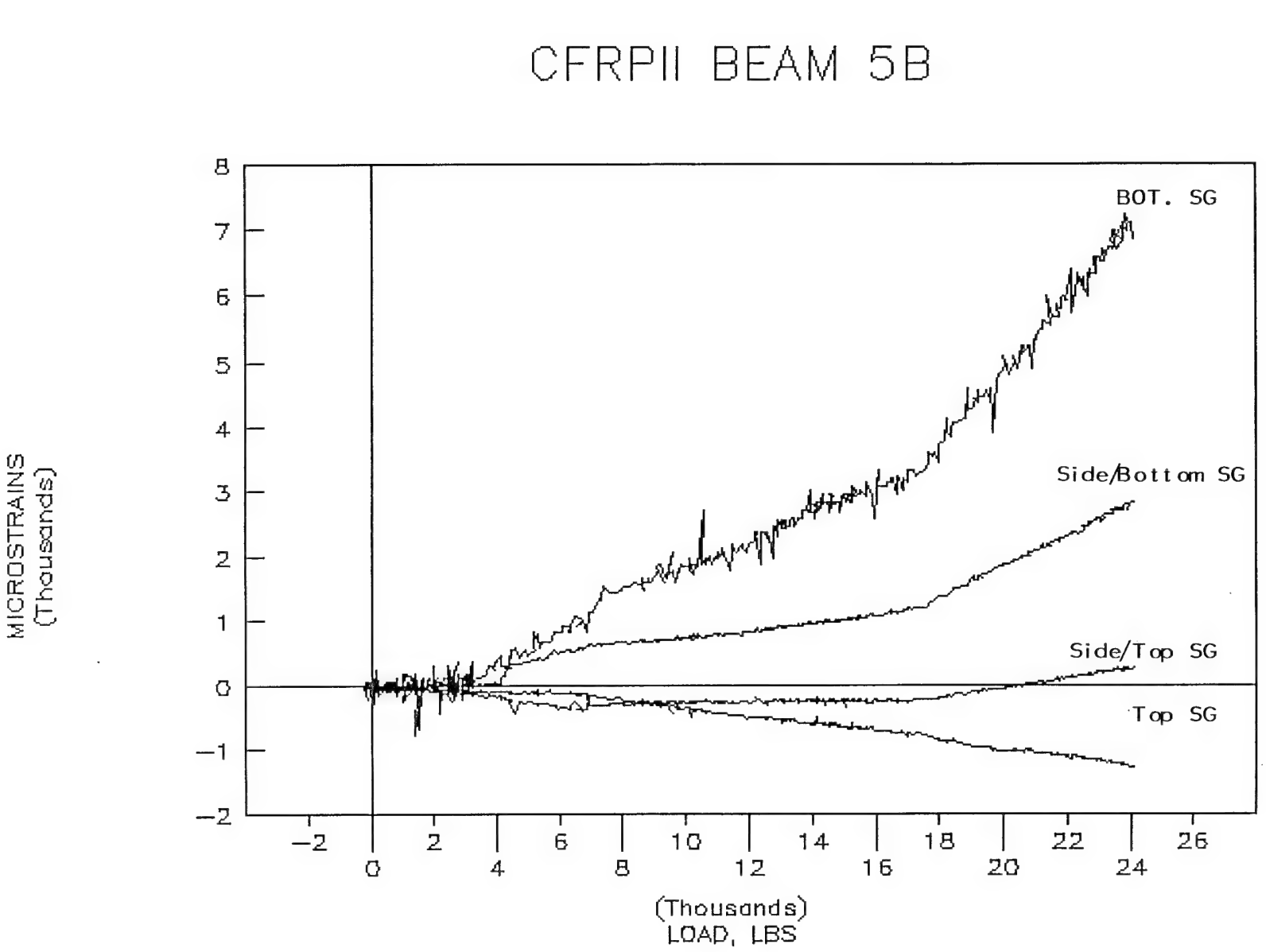

Figure 7. Strain gauge readings for Beam 5B test.

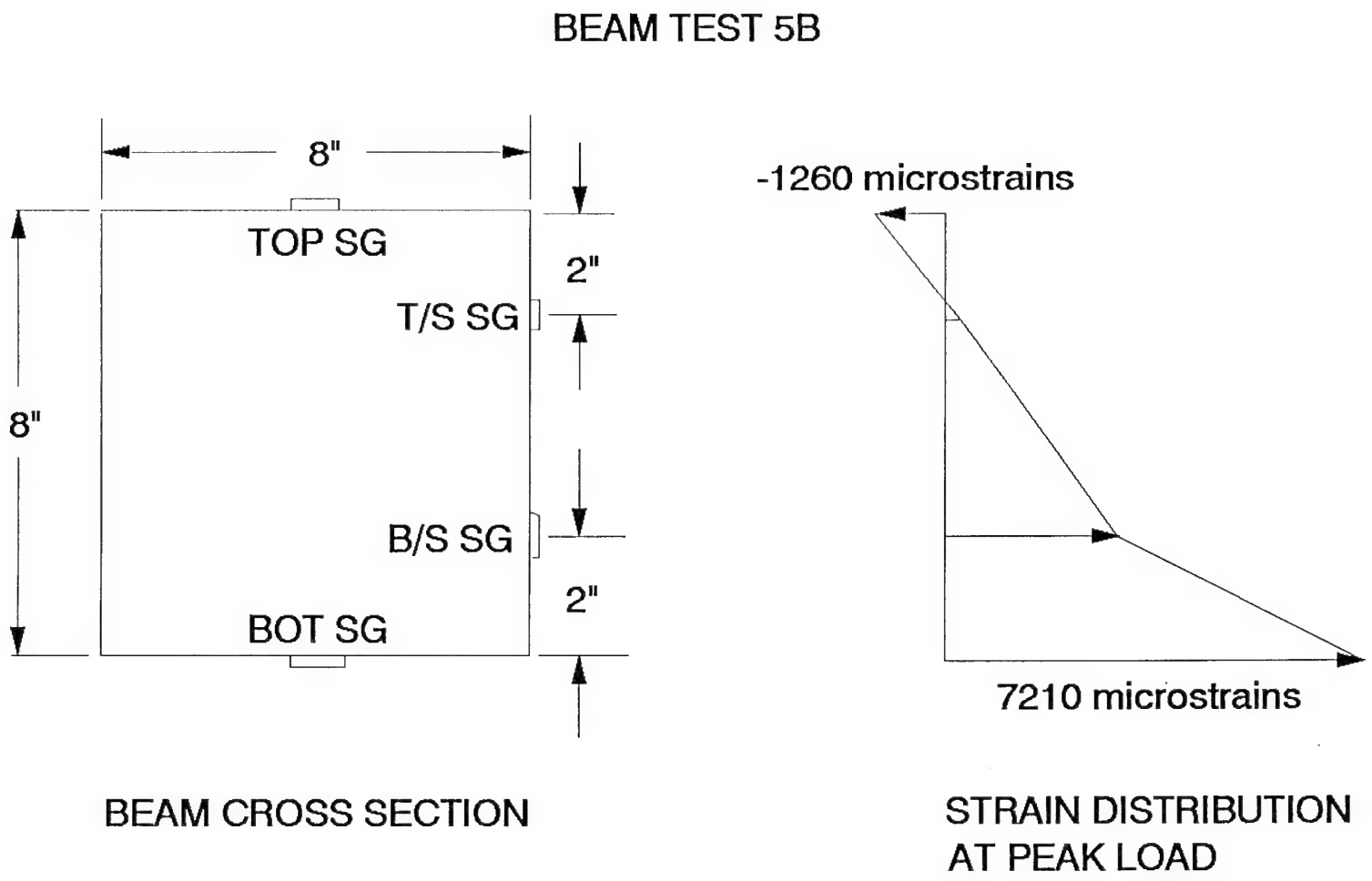

Figure 8. Schematic of beam cross section showing strain gauge placement and strain distribution for beam No. 5.

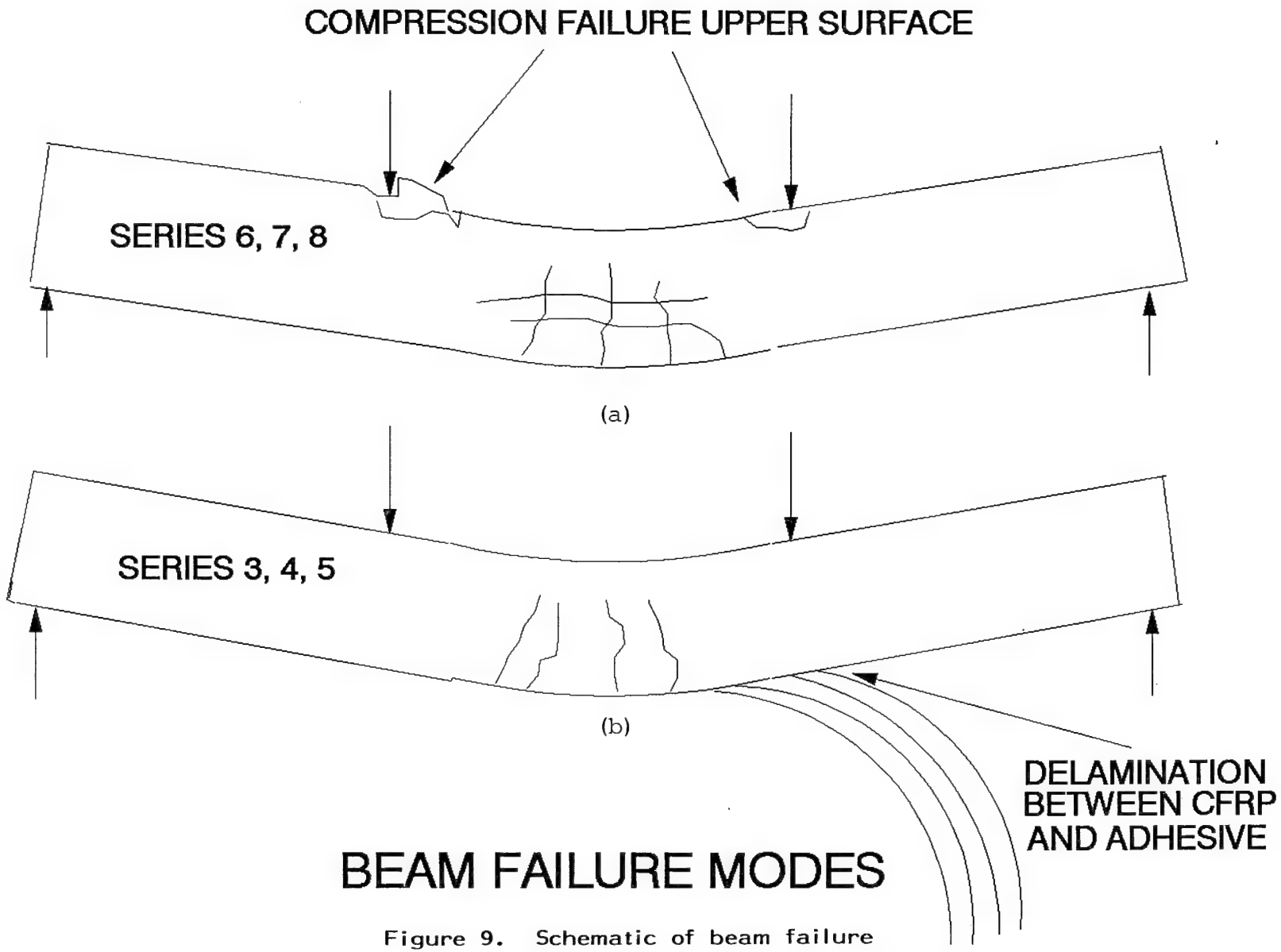

Figure 9. Schematic of beam failure
a) Crushing of compression concrete
b) Delamination of CFRP between CFRP and adhesive

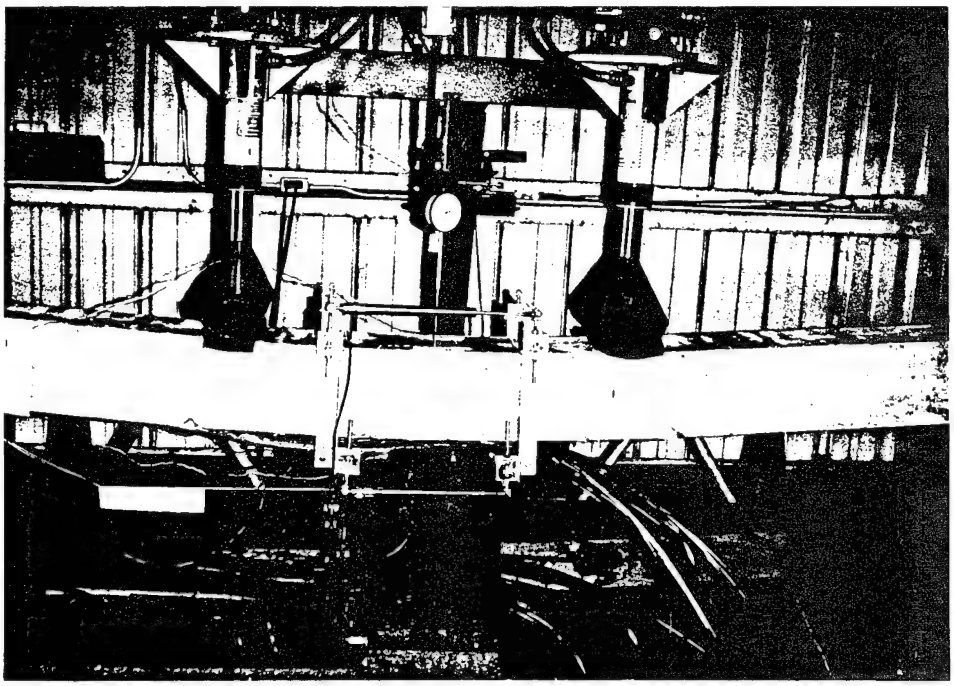

Figure 10. Photograph of beam failure by delamination for a Series 3 beam.

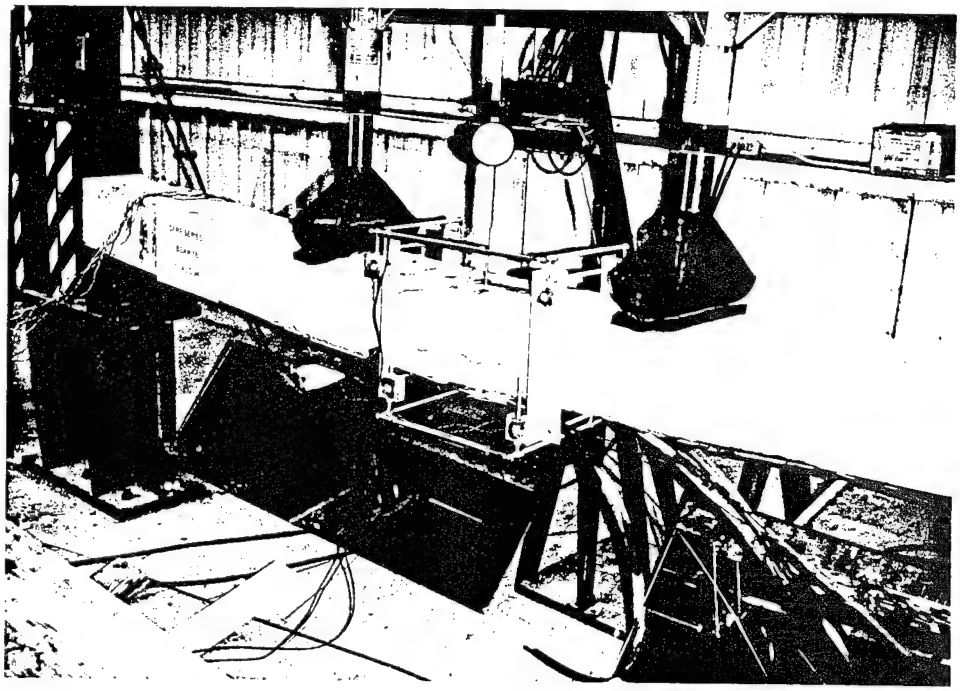

Figure 11. Photograph of beam failure by delamination for a Series 5 beam.

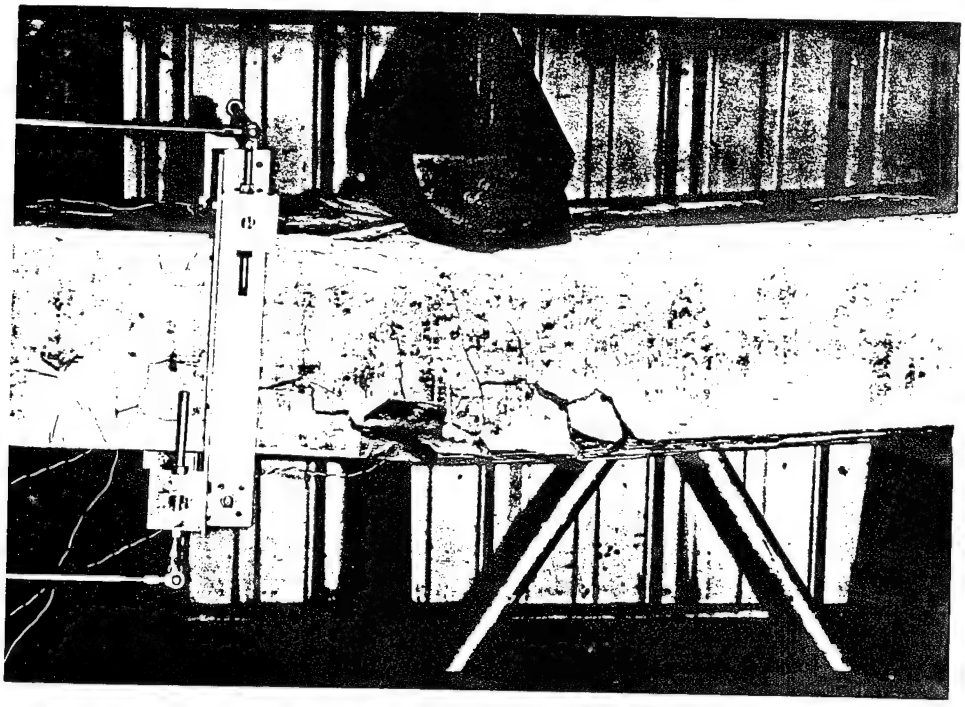

Figure 12. Photograph of beam failure by concrete compression of a Series 6 beam.

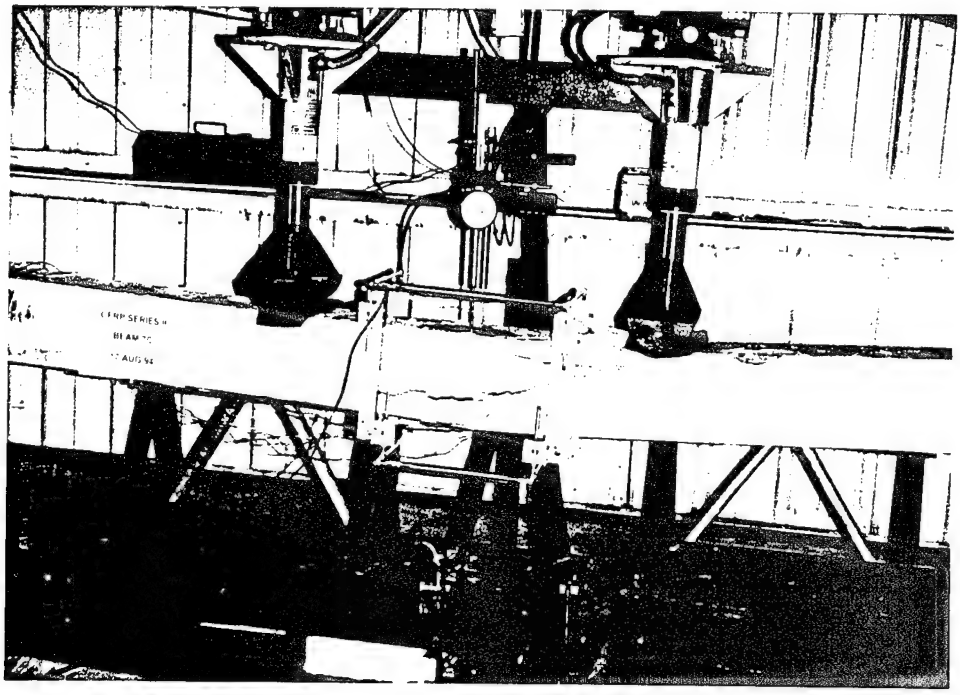

Figure 13. Photograph of beam failure by concrete compression of a Series 7 beam.

Section III

BEAM RESPONSE ANALYSIS

1. Introduction

Analytical calculations for concrete beams using CFRP are based on an elastic/plastic section analysis. Section analysis in this report is based on a composite beam cross-section of concrete, steel, and CFRP. The basic assumption is that the tensile concrete fractures at a very low load which causes a rather large shift in the neutral axis. This neutral axis shift is calculated and used to determine the remaining composite moment of inertia and stiffness which in turn yields a residual resisting moment. In all calculations the strain distribution is assumed to be linear and rotated planes of the beam cross sections remain plane. The assumption of linear strain up to failure was verified experimentally in small beam and large beam tests of 1993. The analyses were accomplished using the various regions of the load-displacement curve as shown in Figure 14. The fourth region may not have been realized experimentally due to the CFRP strength loss in delamination of the CFRP from the adhesive.

An analysis using a Finite Element Method (FEM) computer code ADINA [9] was also conducted.

2. Beam Section Analysis

a. Introduction and Symbols

This analysis is based on concrete beams conventionally reinforced with steel and externally reinforced on the bottom with a three ply unidirectional carbon fiber reinforced plastic panel (CFRP). The beam cross section is shown in Figure 15. The following symbols, definitions and material properties have been used in the analysis:

ϵ_c concrete compressive strain

ϵ_T concrete tensile strain

ϵ_s steel strain

ϵ_y steel yield strain = .002

ϵ_F CFRP strain

ϵ_c' concrete compressive strain at peak compressive stress = 0.00245

ϵ_u maximum concrete compressive strain = 0.003

E_c compression concrete modulus = 5 x 10^6 psi (34.5 GPa)

$\bar{E}_s$ steel work hardening slope = 1.2 x 10^6 psi (8.3 GPa)

E_s tensile steel modulus = 29 x 10^6 psi (200 GPa)

E_F tensile CFRP modulus = 20 x 10^6 psi (137.9 GPa)

N_s E_s/E_c = 5.8

N_F E_F/E_c = 4.0

f_c concrete compressive stress, psi

f_T peak concrete tensile stress, psi

f_s steel stress, psi

f_F CFRP stress, psi

f_y steel tensile yield stress = 60 ksi (0.41 GPa)

f_c' concrete compressive strength = 7,950 psi (54.8 MPa)

f_{Ft} CFRP tensile strength = 320 ksi (2.21 MPa)

f_r concrete modulus of rupture = $0.12f_c'$ = 954 psi (6.58 MPa) [10]

C concrete compressive force, lb

S_a shear strength, adhesive, psi

S_c concrete shear strength, psi

T_c concrete tensile force, lb

T_s steel tensile force, lb

T_F CFRP tensile force, lb

A_s total tensile steel area, in^2

I moment of inertia, in^4

K beam displacement constant =$1296/23L^3$, $1/in^3$

L_a shear development length, in

c neutral axis location from top of beam, in

h beam depth = 8.0 in (20.32 cm)

d tensile steel location from top of beam = 6.0 in (15.24 cm)

b beam width = 8.0 in (20.32 cm)

t CFRP thickness = 0.0175 in (0.45 mm)

γ empirical constant relating average concrete stress to f_c', $\gamma = 0.85$ [11]

β empirical constant for determining position of concrete force C below top of beam, $\beta = 0.325$ [11]

δ beam displacement at specified stages of loading, in

Δ incremental beam displacement between stages of loading, in

CFRP beam analysis is based on experimental observations of linear strain (plane sections remain plane) and a multilinear load-displacement curve shown schematically in Figure 14. The curve is divided into four numbered regions terminated by a similarly numbered point. These four numbered points plus the origin are then connected by straight lines to form the calculated load-displacement curve. In all cases the strain is assumed linear and the compression steel is neglected. Stress-strain curves for the steel and concrete are shown in Figure 16. The stress-strain curve for the CFRP is assumed linear elastic and is terminated in an abrupt failure at f_{Ft}.

Each of these four regions and their respective terminating points illustrated in Figure 14 are discussed in the following sections.

b. Region 1

In this region all materials are assumed to behave elastically until fracture of concrete in the tension region occurs at the modulus of rupture. Referring to Figure 17 all strains may be written in terms of the concrete strain ϵ_c, at the top (compression face) of the beam, and they become

$$\epsilon_T = \epsilon_c(h-c)/c$$
$$\epsilon_s = \epsilon_c(d-c)/c \qquad (1)$$
$$\epsilon_F = \epsilon_c(h-c)/c$$

Since all materials in this region are elastic, the stresses may be expressed as the product of strain times the modulus of elasticity, and the forces acting on the cross section (Figure 17) may be written as

compressive concrete force:

$$C = \epsilon_c E_c bc/2, \qquad (2)$$

tensile concrete force:

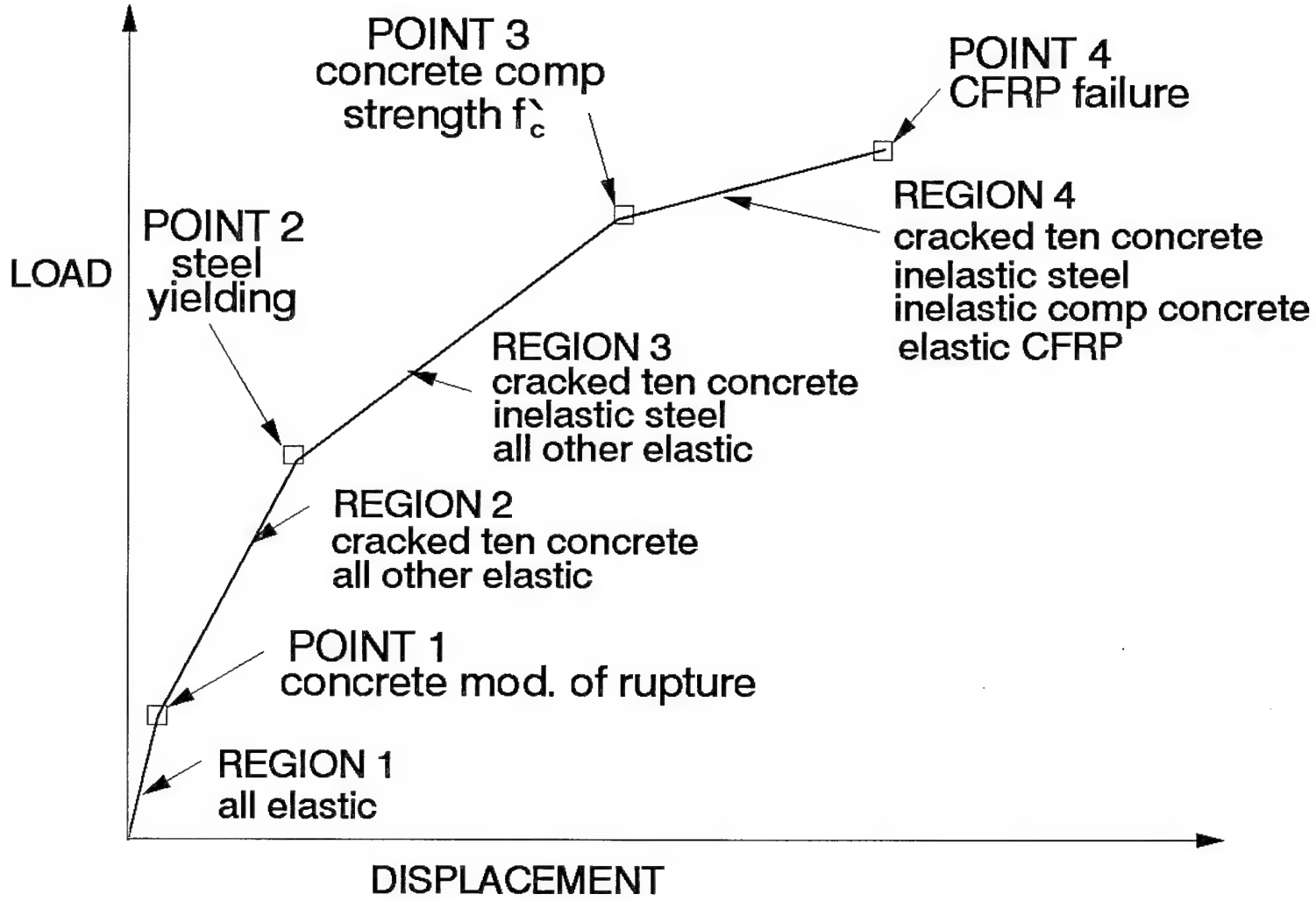

Figure 14. Beam load/displacement response assumptions used in analytical beam section analysis.

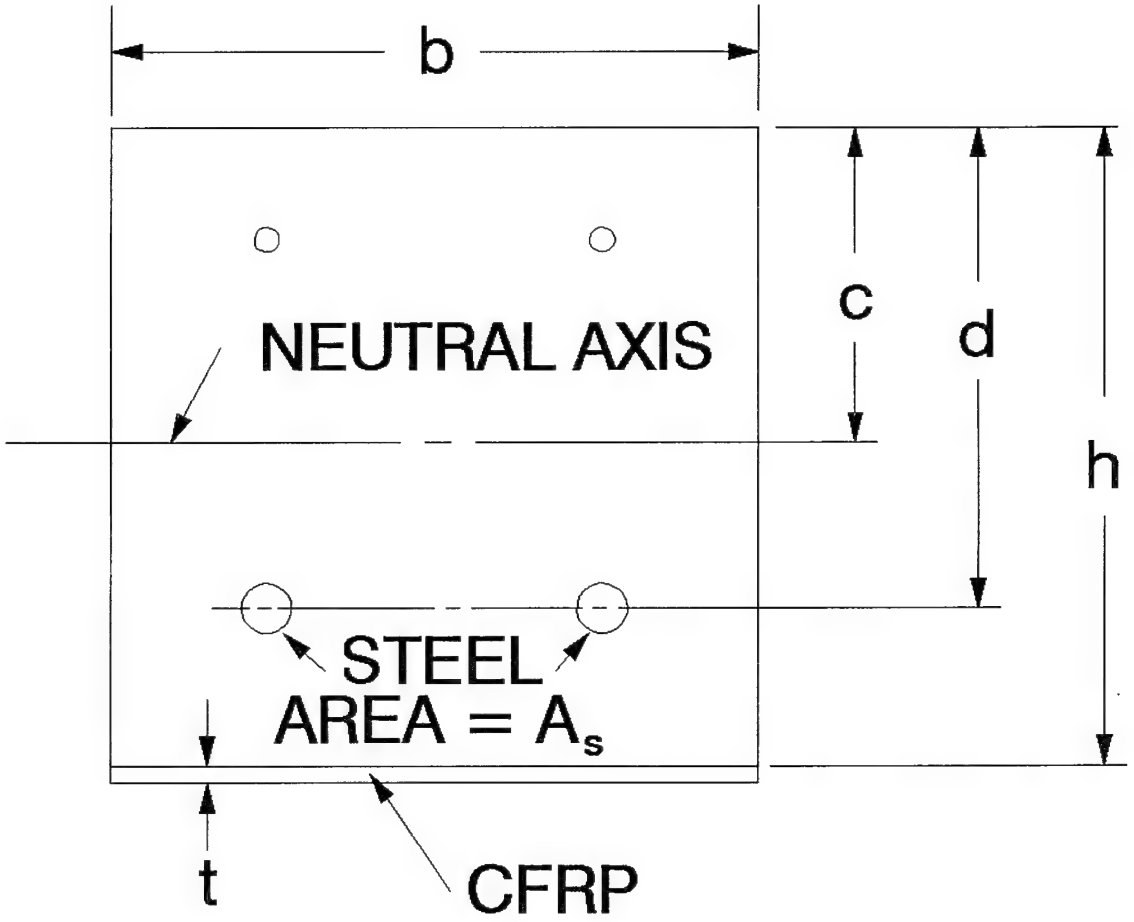

Figure 15. Beam cross section used in all section analyses.

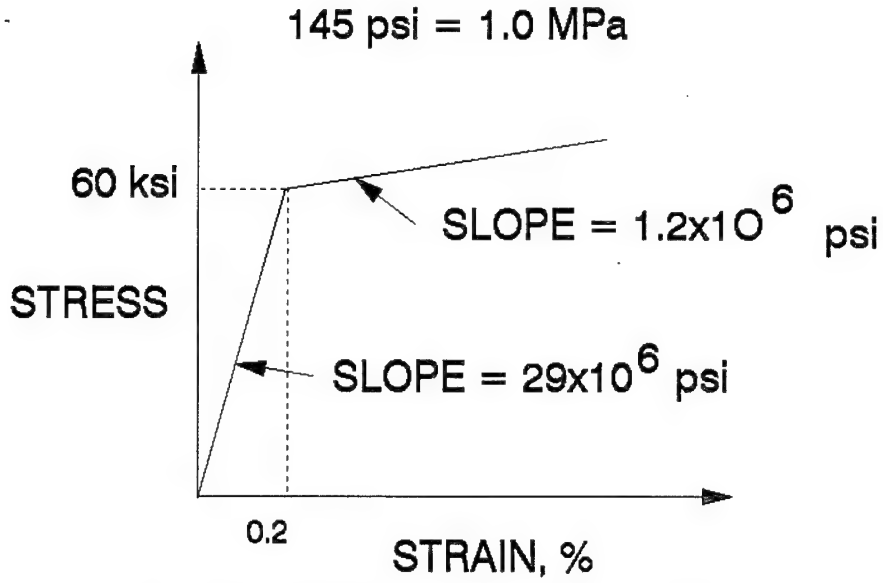

a) Steel tensile stress-strain curves

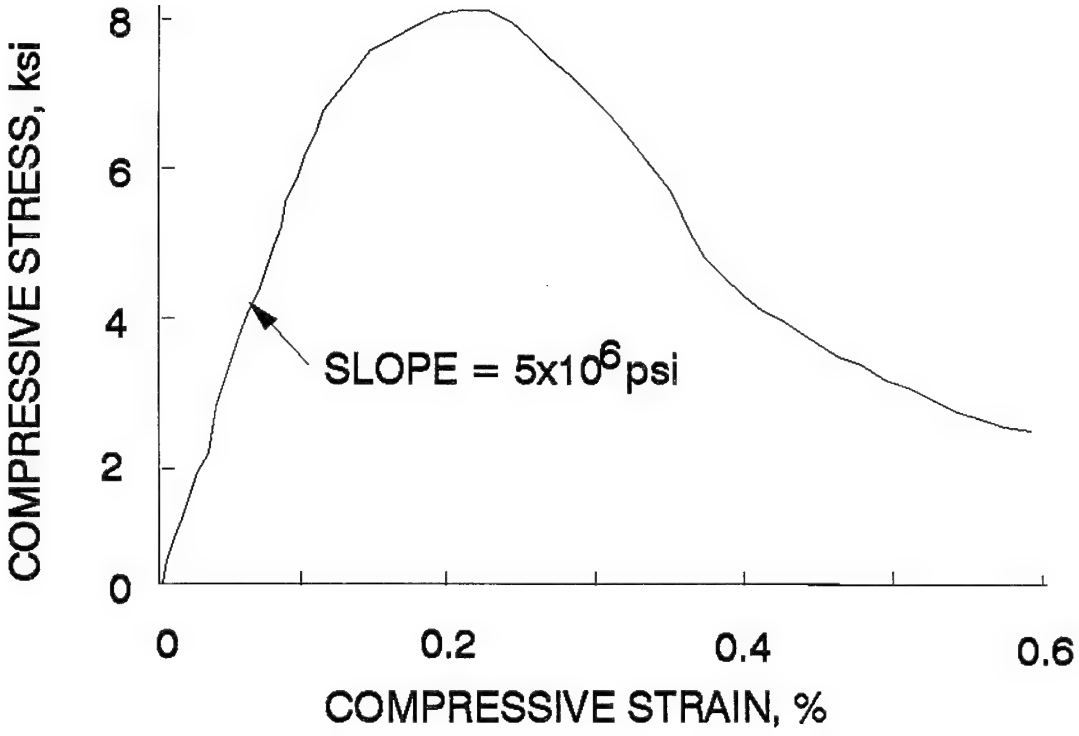

b) Compressive concrete stress-strain curve.

Figure 16. Steel and concrete stress-strain curves used in the section analysis.

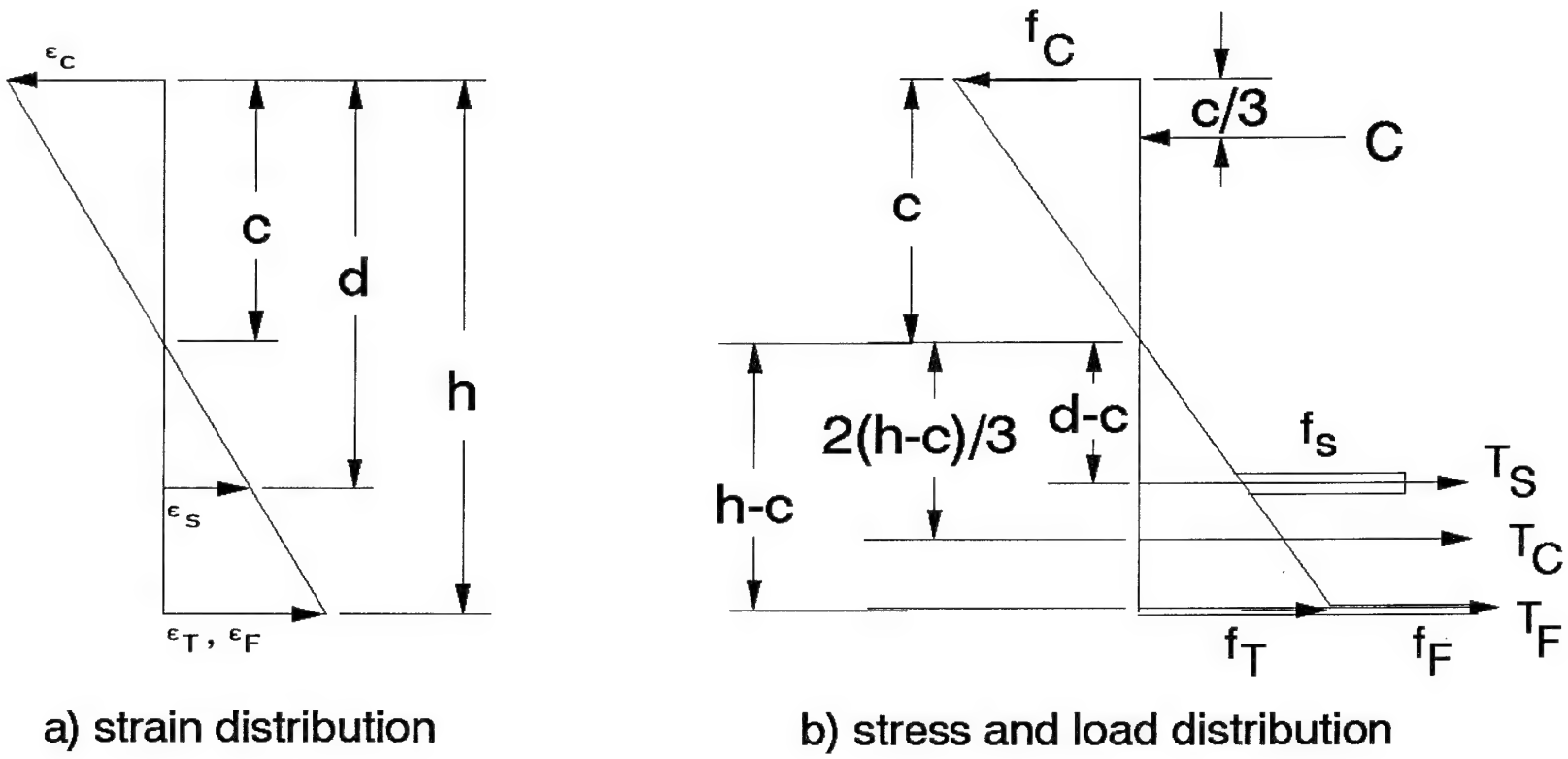

Figure 17. Beam cross section used in Region 1 of the section analysis.

$$T_c = \epsilon_c E_c b(h\text{-}c)^2/2c \quad (3)$$

steel force:

$$T_s = \epsilon_c E_s A_s (d\text{-}c)/c, \quad (4)$$

CFRP force:

$$T_F = \epsilon_c E_F bt(h\text{-}c)/c. \quad (5)$$

Assuming flexural response, the sum of the normal forces acting on the cross section of the beam is zero. This condition is stated as

$$\sum F = C - T_c - T_s - T_F = 0. \quad (6)$$

Substituting Equations (2) - (5) into Equation (6) and dividing each term by $\epsilon_c E_c$ gives

$$c^2 - (h\text{-}c)^2 - 2\,N_s A_s (d\text{-}c)/b - 2N_F t(h\text{-}c) = 0, \quad (7)$$

which results in a linear equation with c and when solved yields

$$c = \frac{h^2 + 2N_s A_s d/b + 2N_F th}{2h + 2N_s A_s/b + 2N_F t}. \quad (8)$$

The slope of the Region 1 curve may be written as

$$(P/\delta)_1 = K(EI)_1 \quad (9)$$

where $(EI)_1$ is the bending stiffness and $K = 1296/23L^3$ is the constant obtained in the derivation of mid-point displacement for the third-point bending used in the static tests. The I term of the bending stiffness is the moment of inertia of the elastic portions of the beam cross section.

Having determined the neutral axis location c, the bending stiffness can be written as

$$(EI)_1 = E_c\, bc^3/3 + E_c b(h\text{-}c)^3/3 + E_s A_s (d\text{-}c)^2 + E_F bt(h\text{-}c)^2, \quad (10)$$

and the moment of inertia of the composite section is determined from the relation

$$I_1 = (EI)_1/E_c. \quad (11)$$

The bending moment M_1 and corresponding load P_1 are related thru the relation for the third-point bending as

$$M_1 = P_1 L/6 \quad (12)$$

and are determined using the modulus of rupture relation

$$f_r = M_1(h\text{-}c)/I_1 = P_1 L(h\text{-}c)/6I_1 \quad (13)$$

$$\delta_1 = P_1/(P/\delta)_1. \tag{14}$$

With this the Point 1 is determined as P_1, δ_1.

c. Region 2

For this region the assumption is that the concrete below the neutral axis is cracked and not active in bending. Referring to Figure 18, the concrete tensile stress T_c of Equation (3) and (6) goes to zero and the second term of Equation (7) disappears resulting in a quadratic equation in c given as

$$c^2 + 2(N_sA_s/b + N_Ft)c - 2(N_sA_sd/b + N_Fth) = 0. \tag{15}$$

In this Region 2 the bending stiffness $(EI)_2$ is determined using Equation (10) with the second term equal to zero. From this the slope of the load-displacement curve for this region is

$$(P/\delta)_2 = K(EI)_2 \tag{16}$$

In order to determine the bending moment M_2 and load P_2, the steel strain ϵ_y at yielding, as shown in Figure 18a, is used to determine the concrete strain ϵ_c and CFRP strain ϵ_F. These strains may be written as

$$\epsilon_c = \epsilon_y c/(d-c)$$
$$\epsilon_F = \epsilon_y(h-c)/(d-c) \tag{17}$$

with steel yielding, $f_s = f_y$, and the forces illustrated in Figure 18b become

$$C = \epsilon_y E_c bc^2/2(d-c) \tag{18}$$

$$T_s = f_y A_s \tag{19}$$

$$T_F = \epsilon_y E_F bt(h-c)/(d-c) \tag{20}$$

Using the neutral axis position c and summing moments about this position, the moment M_2 is found to be

$$M_2 = \epsilon_y E_c bc^3/3(d-c) + f_y A_s(d-c) + \epsilon_y E_F bt(h-c)^2/(d-c) \tag{21}$$

With M_2 known the load P_2 becomes

$$P_2 = 6M_2/L \tag{22}$$

Knowing P_1 and P_2, the increase in displacement from Point 1 to Point 2 is determined from

$$\triangle_2 = (P_2 - P_1)/(P/\delta)_2 \tag{23}$$

and δ_2 becomes

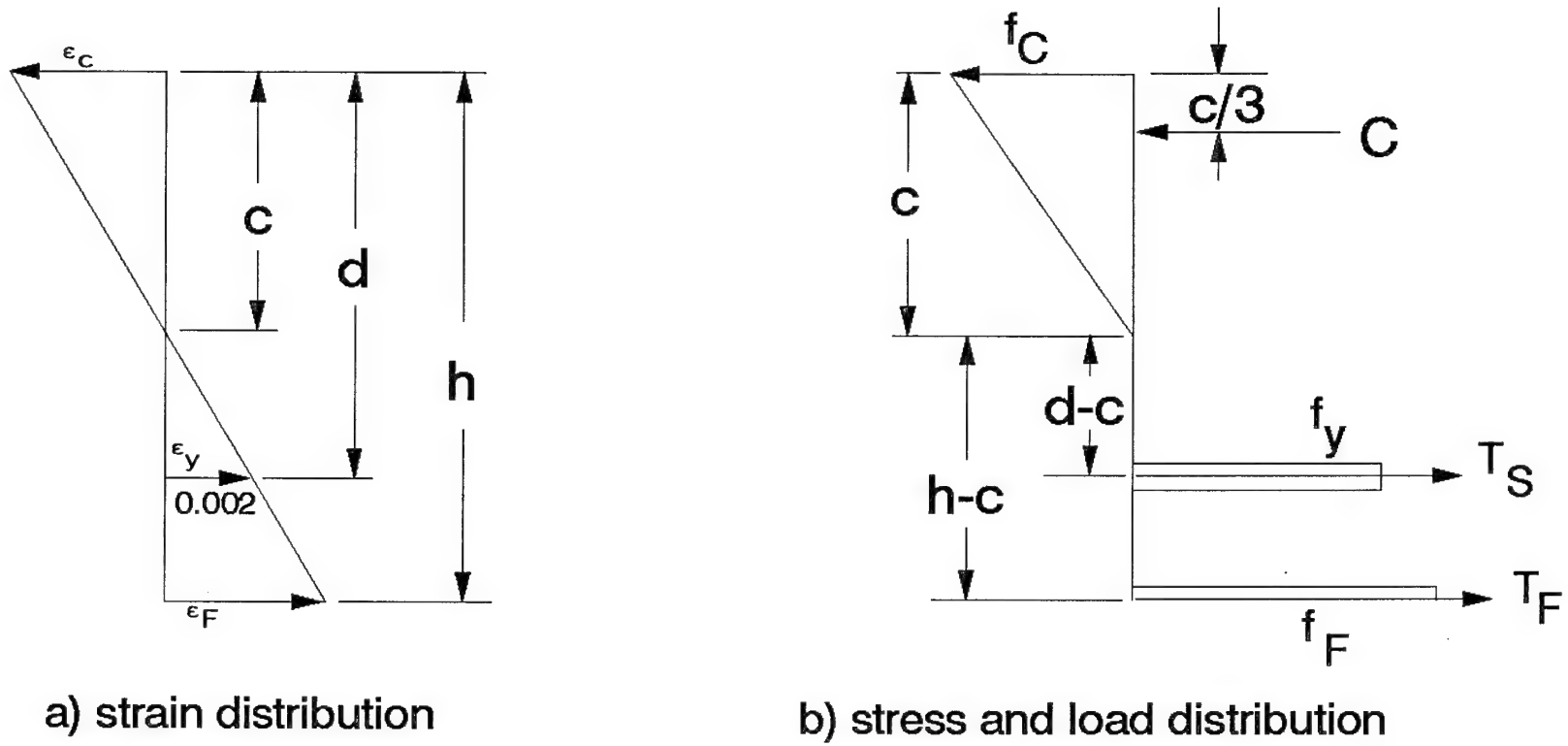

Figure 18. Beam cross section used in Region 2 of the section analysis.

$$\delta_2 = \delta_1 + \triangle_2. \tag{24}$$

d. Region 3

In this region the steel is inelastic having reached the work hardening portion of the stress-strain curve shown in Figure 16a. At the end of this region (Point 3) the concrete will have reached its peak value of f_c and associated strain of ϵ_c, as illustrated in Figure 16b. Using these values as indicated in Figure 19 the strains in the CFRP and steel become

$$\epsilon_F = \epsilon_c(h-c)/c$$
$$\epsilon_s = \epsilon_c(d-c)/c \tag{25}$$

and the forces C, T_s, T_F may be written as

$$C = f_c bc/2$$
$$T_s = [f_y + (\epsilon_s - \epsilon_y)E_s]A_s \tag{26}$$
$$T_F = \epsilon_c E_F bt(h-c)/c.$$

Summing these forces and setting the sum equal zero, results in a quadratic equation in c of

$$f_c'bc^2 - 2[f_yA_s - \epsilon'_c(E_Fbt + \bar{E}_sA_s) - \epsilon_y\bar{E}_sA_s]\,c - 2\epsilon'_c(A_s\bar{E}_sd + bthE_F) = 0 \tag{27}$$

With c known from Equation (27) the moment about the neutral axis M_3 is determined as

$$M_3 = \frac{f_c'bc^2}{3} + (f_y + (\varepsilon_s - \varepsilon_y)E_s)A_s(d-c) + \epsilon_c'E_Fbt(h-c)^2/c \tag{28}$$

and the load P_3 is determined from

$$P_3 = 6M_3/L. \tag{29}$$

Again the bending stiffness for the elastic portions of the beam in Region 3 becomes

$$(EI)_3 = E_cbc^3/3 + E_fbt(h-c)^2 + \bar{E}_sA_s(d-c)^2 \tag{30}$$

The slope of the load/deflection curve is determined from the relationship

$$(P/\delta)_3 = K(EI)_3 \tag{31}$$

and the incremental increase in displacement from Point 2 to Point 3 is determined by

$$\triangle_3 = (P_3 - P_2)/(P/\delta)_3. \tag{32}$$

The total displacement at the Point 3 becomes

$$\delta_3 = \delta_2 + \triangle_3 \tag{33}$$

e. Region 4

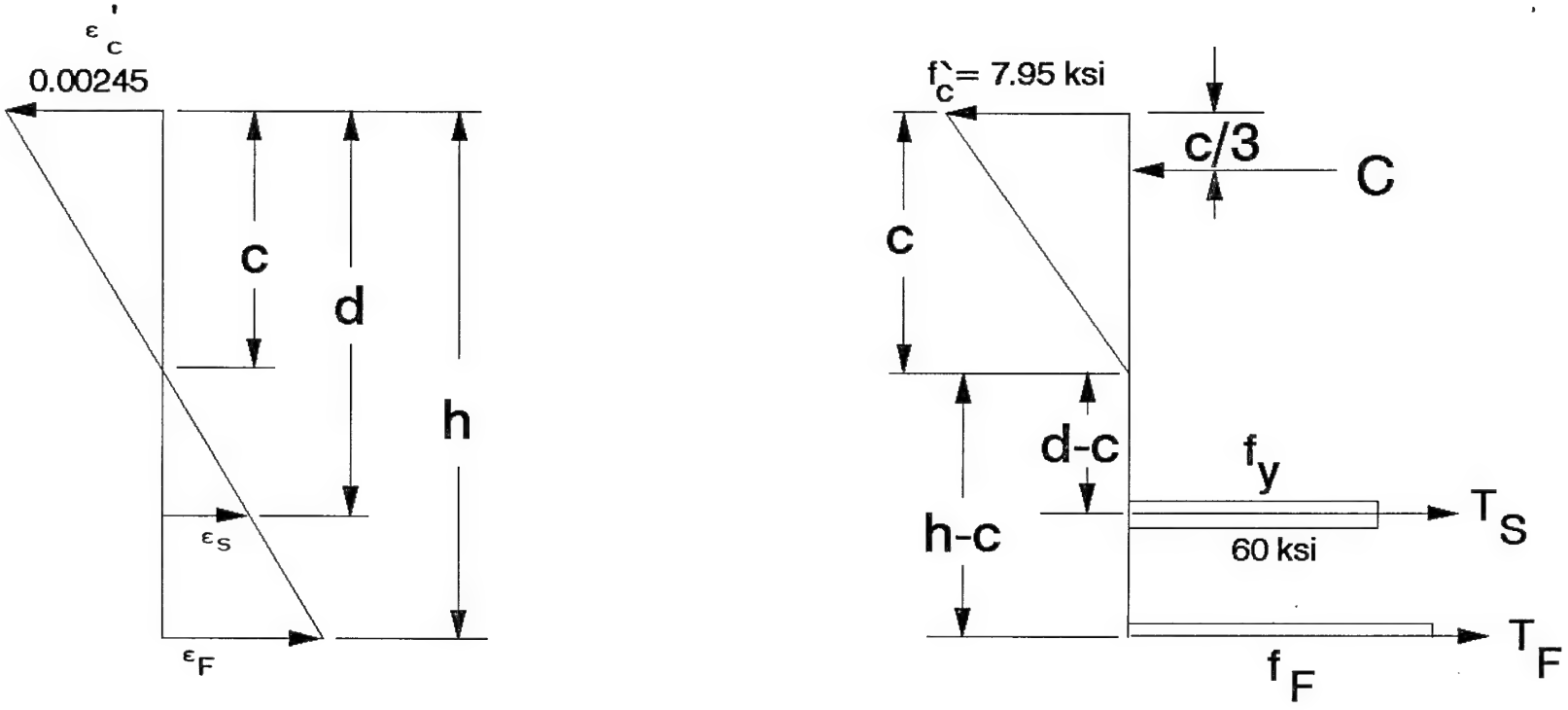

Figure 19. Beam cross section used in Region 3 of the section analysis.

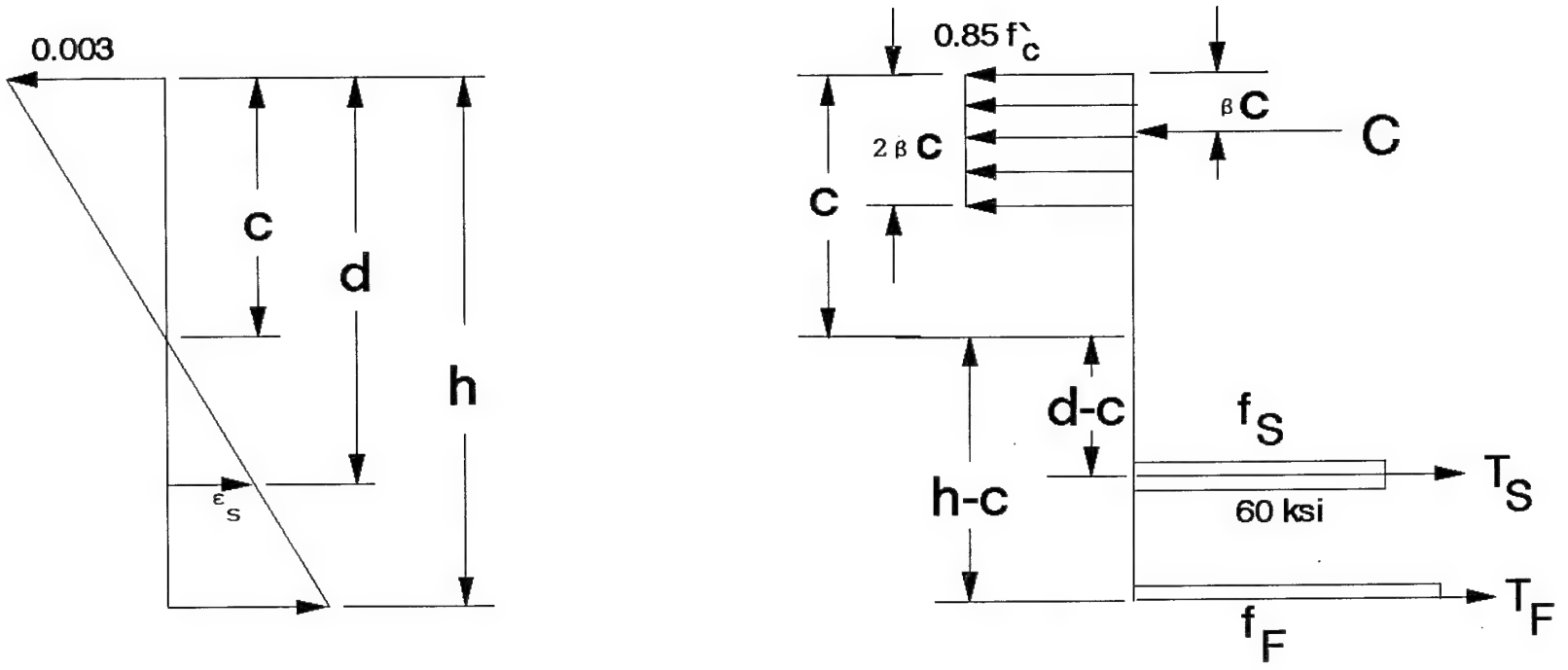

Figure 20. Beam cross section used in Region 4 of the section analysis.

In Region 4, in order to determine a neutral axis position, the concrete compression stress distribution is based on an equivalent rectangular distribution as described by Winter and Nilson [11]. This equivalent stress distribution shown in Figure 20 uses some empirical parameters α, β to describe the equivalent concrete force C and its position relative to the top of the beam. These parameters are based only on f_c and the numerical values are approximately $\alpha = 0.56$ and $\beta = 0.325$ [11]. The position of the concrete compression force C is shown in Figure 20 and its magnitude is given as

$$C = 2\beta\gamma f_c' bc \tag{34}$$

In addition to the equivalent concrete compressive stress distribution, it is also assumed that the concrete strain at the compression face of the beam will have reached some strain ϵ_u of approximately 0.003. This assumption establishes a known parameter needed to determine the strain ϵ_F of the CFRP. Using the experimentally observed linear strain distribution, even at peak beam response, the strains in the CFRP and steel become

$$\epsilon_F = \epsilon_u(h-c)/c$$

$$\epsilon_s = \epsilon_u(d-c)/c. \tag{35}$$

Assuming the steel is still yielding and has not reached its ultimate strain the additional forces T_s and T_F may be written as

$$T_s = [f_y + (\epsilon_s - \epsilon_u) E_s]A_s$$

$$T_F = \epsilon_u E_F bt(h-c)/c \tag{36}$$

Summing the forces C, T_s, T_F results in a quadratic equation in c of

$$2\gamma\beta f_c' bc^2 + [\epsilon_u(E_s A_s + E_F bt) + (\epsilon_y E_s + f_y)A_s]c - \epsilon_u(E_s dA_s + E_F bth) = 0. \tag{37}$$

In this Region 4 concrete crushing may occur prior to failure of the CFRP or the CFRP may debond due to inadequate strength between the CFRP and adhesive or low shear strength at the concrete-adhesive interface. All of this affects the position of the neutral axis. However, the calculated position of the neutral axis does not change significantly as the strain ϵ_u varies from 0.003 to .005, along with the changes of the CFRP stress f_F from 180 ksi to 300 ksi (1.24 GPa to 2.07 GPa).

Calculation of ultimate bending moments, loads and displacement of concrete reinforced only with steel is in itself difficult and not very straight forward and accurate. Increasing the difficulty by adding CFRP simply compounds the problem. With this in mind, the assumptions are made that the neutral axis is based on Equation (37), and the compressive concrete strain is allowed to increase while the concrete resisting force C is a constant based on f_c'.

The moment M_4 is based on a constant compressive resisting concrete force C, a steel tensile force T_s, and a CFRP force T_F which depends on the tensile strength f_F developed in the CFRP. The moment M_4 is used here to determine the slope of the line of the region 4. The load P_4 is not expected to reach its calculated value but serves to determine the slope beyond Point 3. Using this assumption, T_F becomes

$$T_F = f_F bt, \tag{38}$$

and the bending moment becomes

$$M_4 = 2\gamma f_c' bc^2(1-\beta) + [\, f_y + \bar{E}_s \epsilon_c (d-c)/c - \bar{E}_s \epsilon_y](d-c)\, A_s + f_F bt(h-c) \tag{39}$$

Bending stiffness for this region is based on the CFRP panel and the steel work hardening. In reality this bending stiffness only defines the slope of the load-deflection curve above the Point 3 and is given as

$$(EI)_4 = E_f bt(h-c)^2 + \bar{E}_s A_s (d-c)^2. \tag{40}$$

From M_4 of Equation (39) the load P_4 becomes

$$P_4 = 6M_4/L \tag{41}$$

and the load-displacement slope is

$$(P/\delta)_4 = K(EI)_4 \tag{42}$$

Using Equation (42) the increase in displacement from Point 3 is

$$\triangle_4 = P_4/(P/\delta)_4 \tag{43}$$

and the displacement at Point 4 becomes

$$\delta_4 = \delta_3 + \triangle_4. \tag{44}$$

The results of these analyses gives four points plus the origin which, when plotted, give a multilinear load-displacement curve.

3. Analytical Results and Discussion

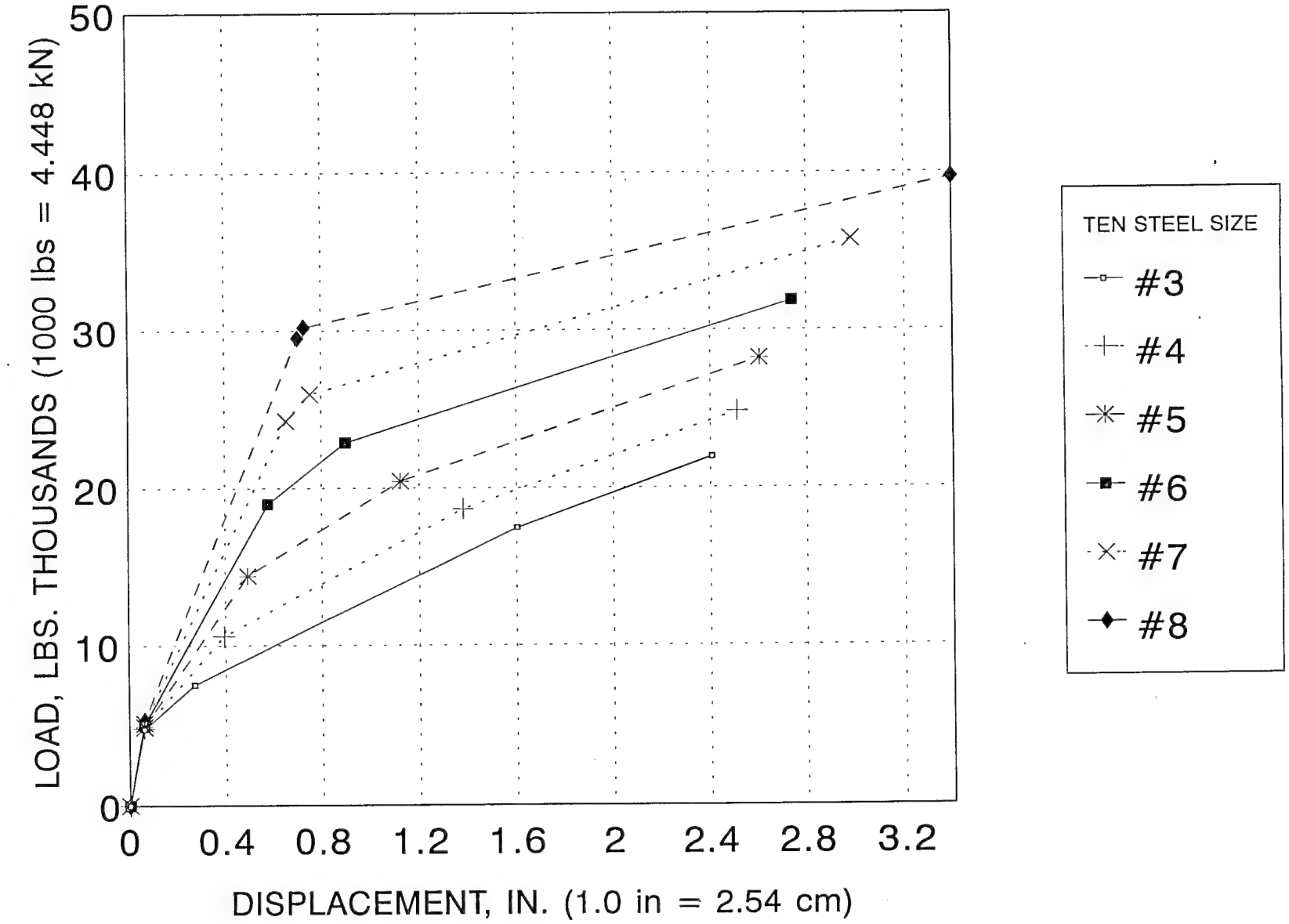

Figure 21. Calculated load-displacement curves using section analysis.

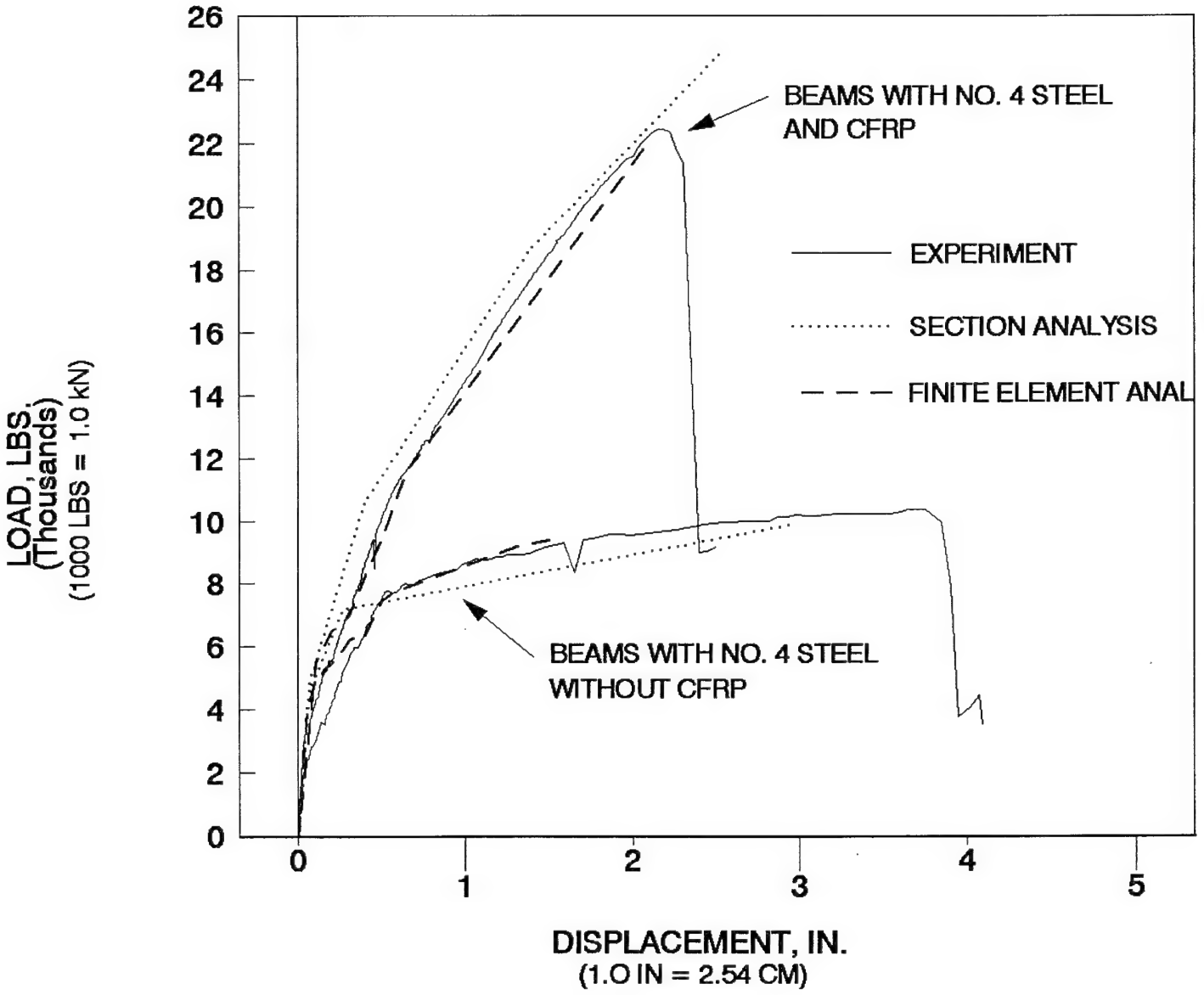

Figure 22. Comparison of calculated and experimental curves for the No. 4 beam series.

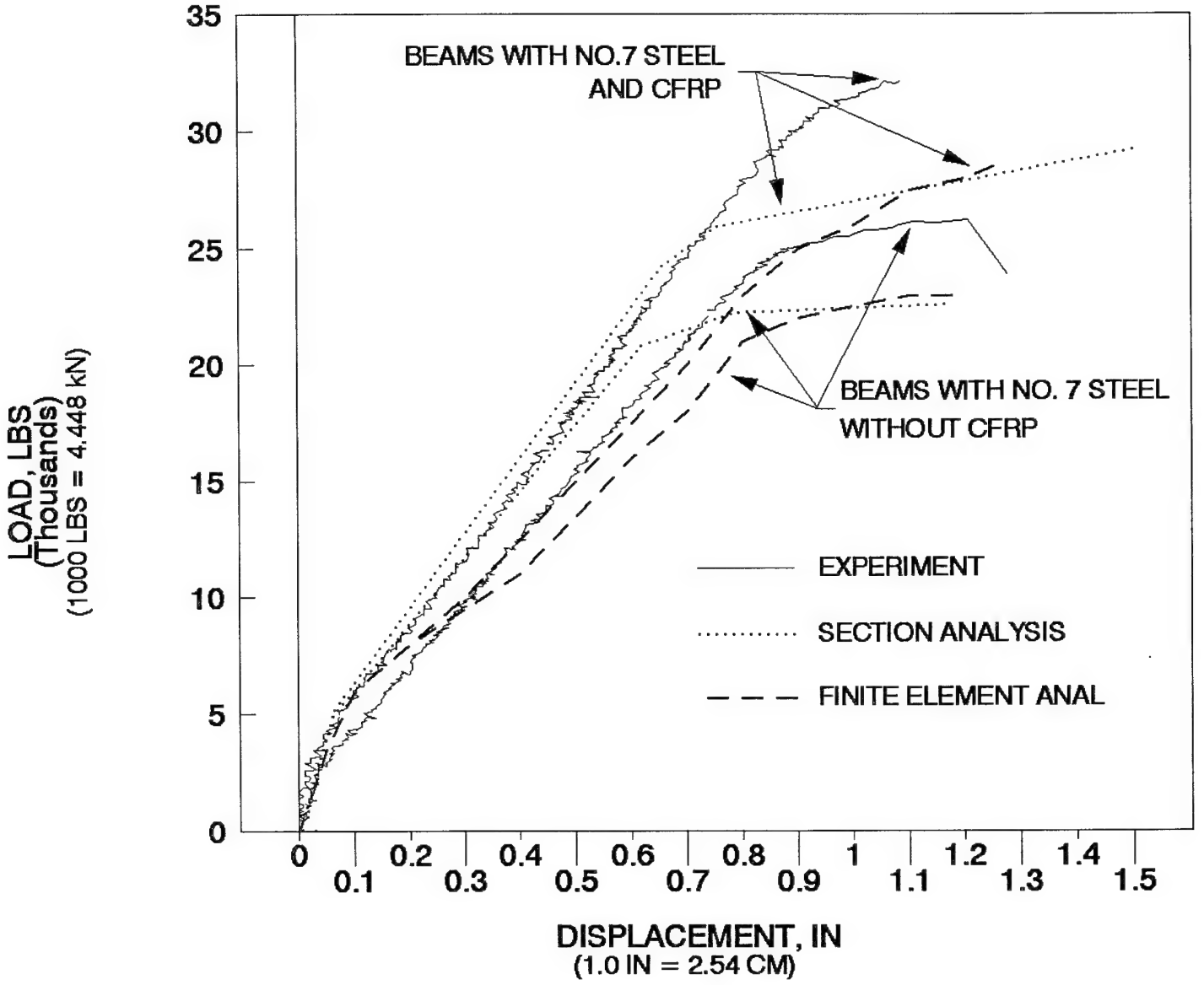

Figure 23. Comparison of calculated and experimental curves for the No. 7 beam series.

As stated in Section II.3 the experimental results were given in English units. In order that comparisons may be made the analytical and numerical results are also given in English units with proper notation to convert to SI units.

The results of the section analysis for the given steel bar sizes of No. 3 to No. 8 are shown in Figure 21. A comparison between experiment and analysis is shown for beam series No. 4 and No. 7 in Figures 22 and 23, respectively. Reasonable agreement between analysis and experiment is shown in these curves. It appears that the Region 4 is not attained in the experimental results. This may be attributable to delamination at lower steel reinforcement and upper surface concrete failure at higher steel reinforcement which results in the inability of the beam to properly load the CFRP to its high strength capacity.

Experimentally the peak strain reached in the CFRP was approximately 8000 microstrains and when multiplied by the modulus of 20×10^6 psi (138 GPa) gives a peak CFRP stress f_F of 160,000 psi (1.1 GPa). It is assumed that this stress is reacted by a shear stress in between the CFRP and the adhesive or as a concrete shear stress between the adhesive and concrete as shown in Figure 24. Assuming an effective shear developement length L_a of twice the beam width 2b and a shear strength of S_a the balance between the CFRP force and the shear force becomes

$$f_F bt = S_a b L_a = 2 S_a b^2 \tag{45}$$

and

$$S_a = f_F t / 2b. \tag{46}$$

Using the given values of f_F, b, and t, the shear stress S_a is approximated as $S_a = 175$ psi (1.21 MPa).

The shear strength S_c for concrete as given in Reference 11 is

$$S_c = 3.5 \, (f_c')^{1/2}$$

and for f_c' of 7950 psi (5.52 MPa) the shear strength between the adhesive and concrete becomes 312 psi (2.15 MPa). This predicts that delamination will occur between the CFRP and the adhesive which is verified experimentally for the No. 3, 4, and 5 series beams.

Using the section analysis to calculate the stress developed in the CFRP, a curve of CFRP stress versus beam applied load is shown in Figure 25. The maximum CFRP stress predicted by experiment is shown as a horizontal line of Figure 25. All beams which reach a CFRP stress higher

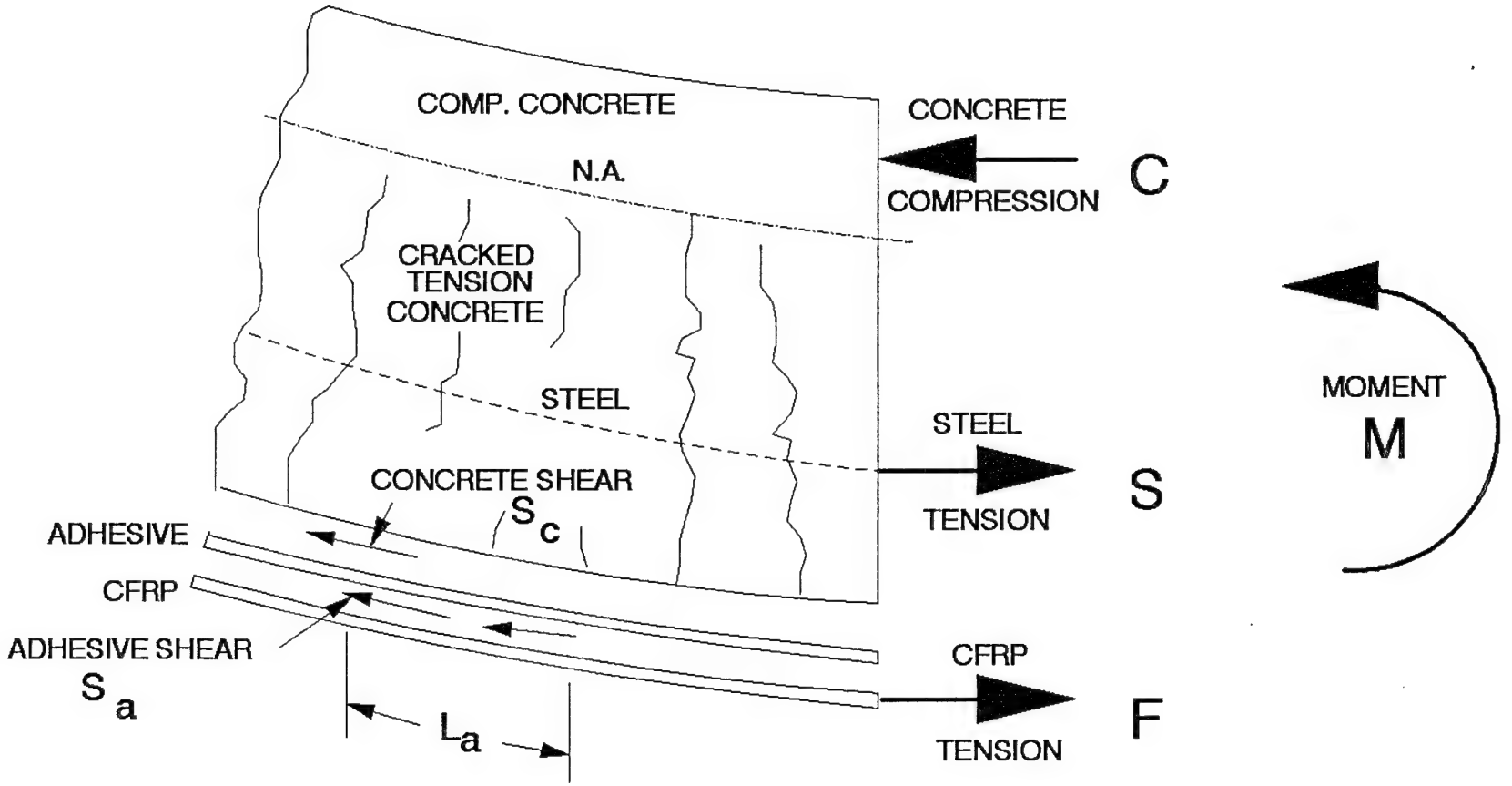

Figure 24. Schematic of internal stresses and loads in a concrete/CFRP beam.

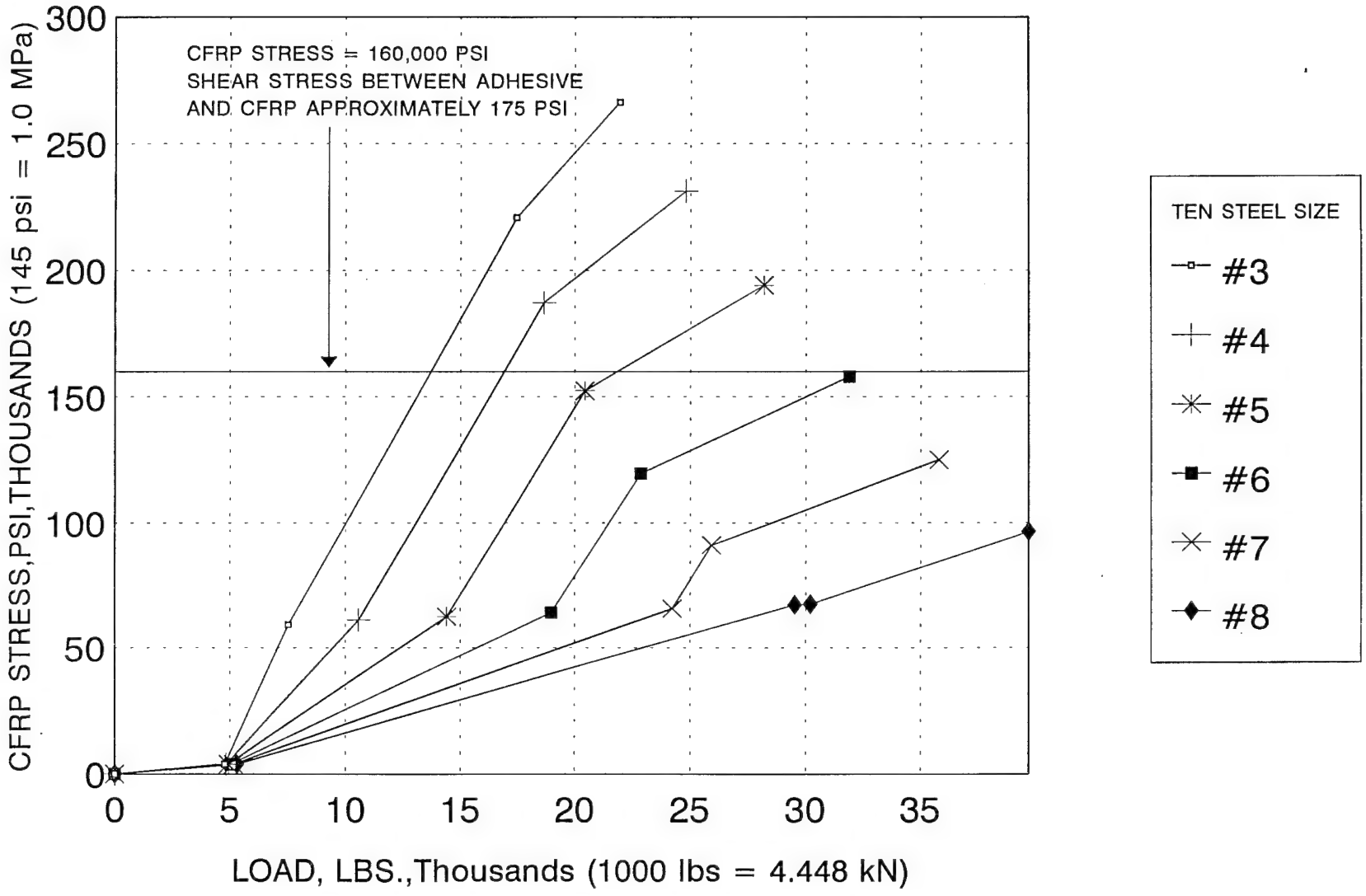

Figure 25. Calculated CFRP stress based on section analysis.

that this line should fail by delamination and those below this line should fail by concrete compression of the upper surface. Results of this curve showing that Beam Series 3, 4, and 5 should fail by delamination and Beam Series 6, 7, and 8 should fail by concrete compression verifies the experimental results of the table of page 10.

4. Numerical Results and Discussion

The ADINA [9] finite element computer code was used to calculate the beam response of concrete beams with Nos. 4 and 7 steel reinforcing rods, both with and without CFRP. A hypoelastic concrete material model is used in compression and a linear elastic model with tension cutoff is used for tensile failures. An elastic work hardening tensile steel material model (Figure 16a) and an elastic CFRP material model with a Young's modulus of 20×10^6 psi were used in the numerical analysis. The same properties as cited in Section III, 2a were used in the analysis.

Twenty-seven two-dimensional eight node plane stress elements were used for the concrete. Nine three-node truss elements were used for the steel and the CFRP. As was the case in the section analysis the compression steel was ignored, and the cross sectional area of the steel truss element was adjusted to include both steel rod areas. Also in the case of the CFRP panel the area of the CFRP truss element was taken to be the beam width times the CFRP panel thickness t.

Loads were applied in increments of the following manner;

a) #4 Ten. Steel, No CFRP, 10,500 lbs in 210 steps

b) #4 Ten. Steel, With CFRP, 22,000 lbs in 440 steps

c) #7 Ten. Steel, No CFRP, 26,000 lbs in 520 steps

d) #7 Ten. Steel, With CFRP, 33,000 lbs in 660 steps

A limited amount of output was requested for this study. For each case listed above a plot of concrete cracking shown in the original mesh and a plot of load versus displacement are given in Figures 26 to 29. Figure 26a shows elements of the original mesh along with the crack patterns. This data is omitted in the other concrete cracking plots.

The load displacement curves of Figures 26 - 29 are reproduced in Figures 22 and 23 showing comparisons between experiment, section analysis, and FEM analysis. For Figure 22, with beams containing No. 4 steel bars, the various methods of analyses show excellent agreement between each other. Also each analyses exhibit the three or four response regions shown schematically in Figure14.

For the analyses of beams containing No. 7 steel bars the analyses are not nearly in agreement with the experiment-as the analysis of beams containing No. 4 steel bars.

The FEM analysis required considerable man hours as well as CPU time. The inelastic-tensile response of the concrete cracking causes the load step to be reduced almost down to 1.0 lb increments during the FEM calculation. This means the CPU time may approach two to three hours on the higher loadings of the beams reinforced with No. 7 steel bars. However, it appears the FEM analysis is worthwhile in that it gives a verification of the section analysis and appears to agree very well with the experimental data.

It is still worth repeating here that we cannot predict the failure load of these beams until further study is made to determine the interaction and failure mechanisms in the bond between the CFRP, adhesive, and concrete.

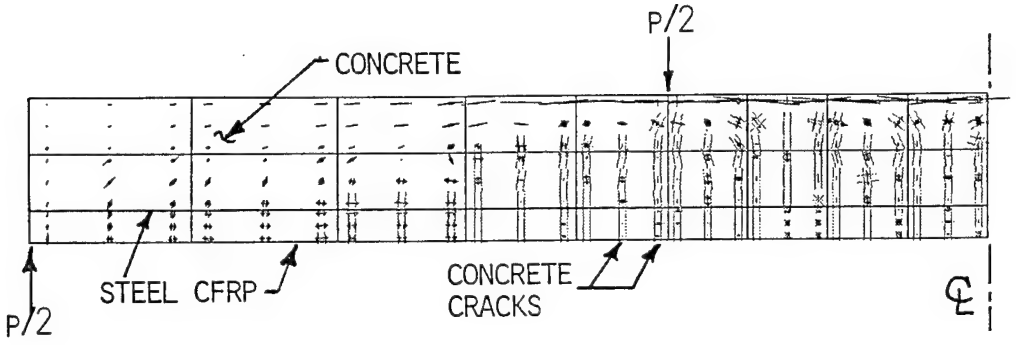

a) crack pattern

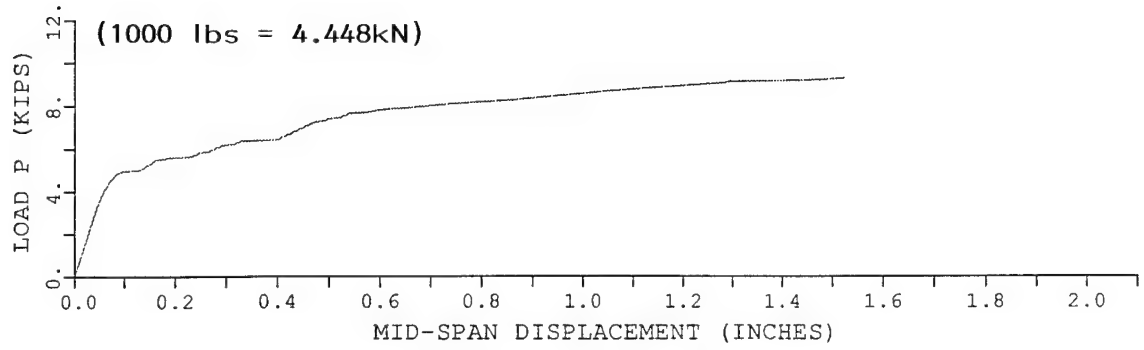

(1.0 in = 2.54 cm)

b) load-displacement

Figure 26. Concrete crack pattern at peak load and load-displacement curve for concrete beams series No. 4 with no CFRP.

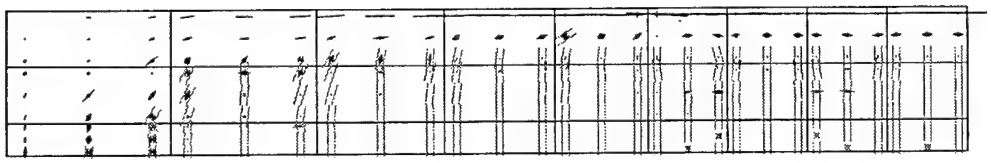

a) crack pattern

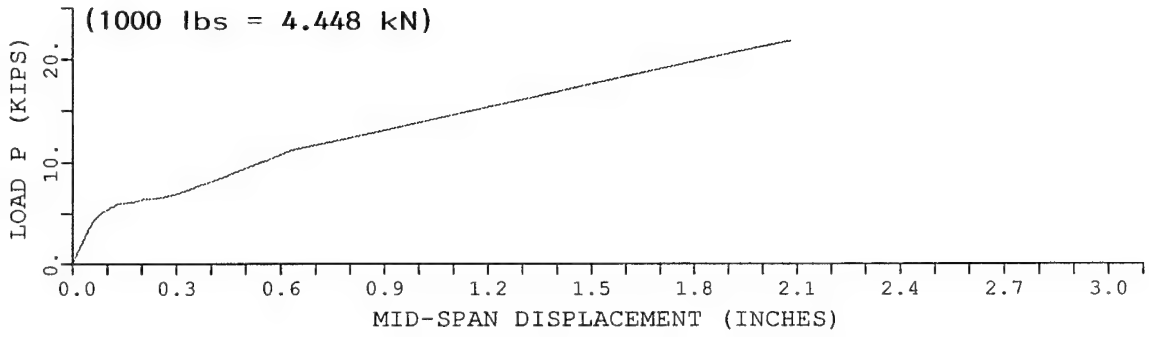

(1.0 in = 2.54 cm)

b) load-displacement

Figure 27. Concrete crack pattern at peak load and load-displacement curve for concrete beam series No. 4 with CFRP.

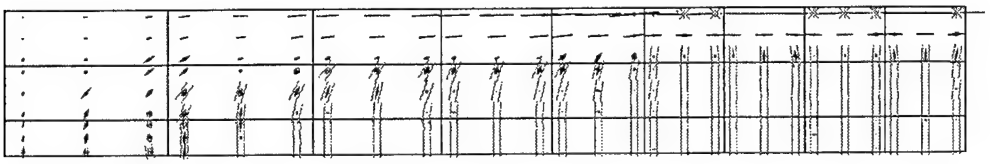

a) crack pattern

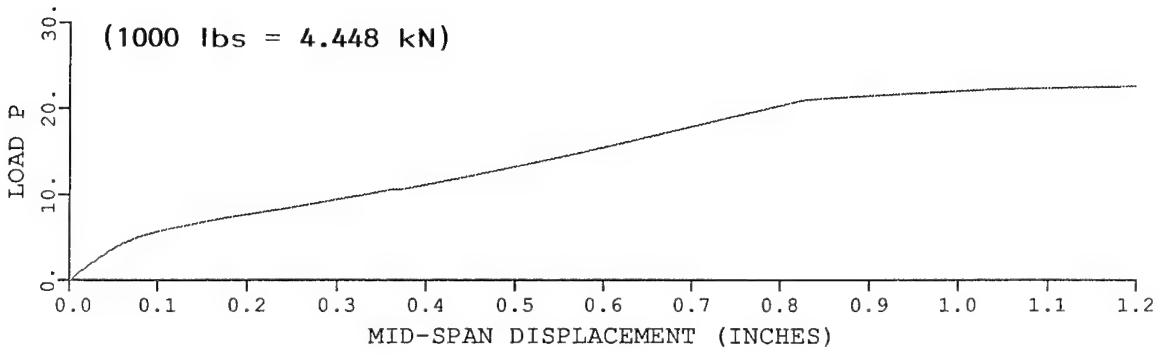

(1.0 in = 2.54 cm)

b) load-displacement

Figure 28. Concrete crack pattern at peak load and load-displacement curve for concrete beam series No. 7 with no CFRP.

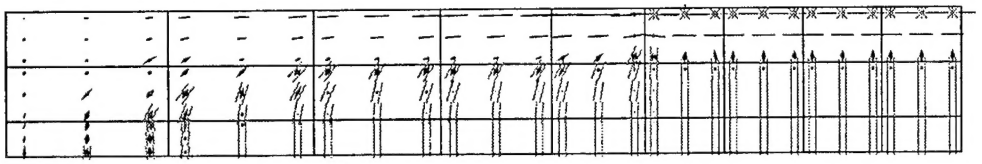

a) crack pattern

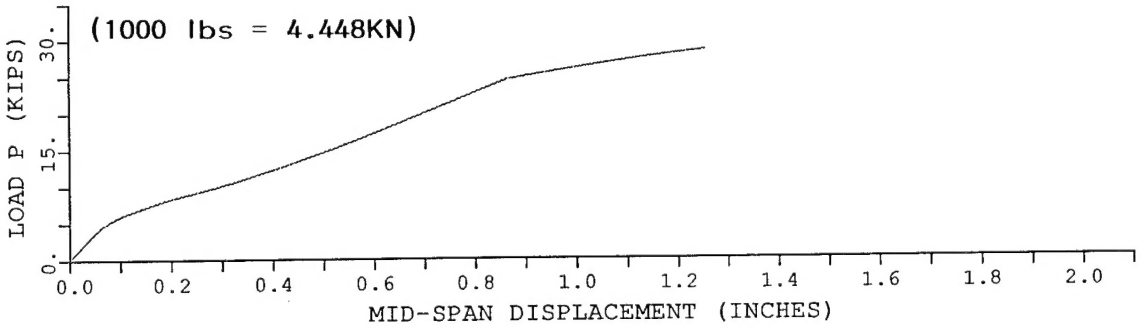

(1.0 in = 2.54 cm)

b) load-displacement

Figure 29. Concrete crack pattern at peak load and load-displacement curve for concrete beam series No. 7 with CFRP.

Section IV

CONCLUSIONS AND RECOMMENDATIONS

The major conclusion from the experimental tests is that a definite strength enhancement is obtained by addition of very thin tensile CFRP panels to concrete beams with conventional steel reinforcement ratios less than approximately one percent. For the concrete/CFRP beams tested, the weakest link appears to be in the shear strength of the adhesive/CFRP interface.

Based on experimental observations the lightly steel reinforced beams respond in a multilinear load-displacement fashion and above the steel yield point, the addition of the CFRP is most effective, accounting for approximately seventy-five percent of the beam stiffness. This leads to the conclusion that the high stiffness of the CFRP may be more important than the high strength. With delamination between CFRP and adhesive and/or low shear strength of the CFRP, is not used to its full potential.

In terms of structural response analysis the recommendation is to expand the analysis to plates and dynamic analysis of both beams and plates.

Finally, the most important overall recommendation is to study the bond strength between both CFRP and adhesive and adhesive and concrete. Studies of both chemical bond strength as well as the mechanics of the interactions between the three parts is essential for increased strength enhancement.

References

1. Meier, U., Deuring, M., Meier, H., and Schwegler, G., Strengthening of Structures with CFRP Laminates: Research and Applications in Switzerland. K. W. Neale and P. Labossiere, Eds., Canadian Society for Civil Eng., 1992, pp. 243 - 251.
2. Meier, U., "Bridge Repair with High Performance Composite Materials," Material und Tichnik, V. 4, 1987, pp. 125 - 128 (in German).
3. Kaiser, H., "Strengthening of Reinforced Concrete with Epoxy-Bonded Carbon-Fiber Panels," Doctoral Dissertation, ETH, 1989 (in German).
4. Triantafillou, T. C., Deskovic, N., and Deuring, M., "Strengthening of Concrete Structures with Prestressed Fiber Reinforced Plastic Sheets," ACI Structural Journal, V. 89, No. 3, May - June 1992, pp. 235 - 244.
5. Sierakowski, R. L., Ross, C. A., Tedesco, J. W., and Hughes, M. L., "Concrete Beams with Externally Bonded Carbon Fiber Reinforced Plastic (CFRP) Strips," Proceedings of ASCE 1994 Materials Engineering Conference, San Diego, CA, Nov. 1994.
6. Shihie, W. and Ruixian, Z., "The Study of Fiber Composite Plates For Strengthening Reinforced Bridges," Proceedings of International Symposium on Concrete Materials in Structures, Beijing, China. Aug. 1992, pp. 224-231.
7. Sharif, A., Al-Sulaimani, G. J., Basunbul, I. A., Baluch, M. H. and Ghaleb, "Strengthening of Initially Loaded Reinforced Concrete Beams Using FRP Plates," ACI Structural Journal, March/April 1994, pp. 160-168.
8. Chajes, M. J., Thomson, T. A. Jr., Januszka, T. F., and Finch, W. W. Jr., "Flexural Strengthening of Concrete Beams Using Externally Bonded Composite Materials," Construction and Building Materials, Vol. 8, No. 3, 1994, pp. 191-201.
9. ADINA, A Finite Element Computer Program for Automatic Dynamic Incremental Nonlinear Analysis, Dept ARD 84-1, ADINA R&D Inc., Watertown, MA, Dec 1984.
10. Neville, A. M., Properties of Concrete, Wiley and Sons, NY, NY, 1973.
11. Winter, G. and Nilson, A. H., Design of Concrete Structures, Ninth Edition, McGraw-Hill Book Co., NY, NY, 1979.

INITIAL DISTRIBUTION
WL-TR-94-7100

Defense Tech Info Center 2
Attn: DTIC-DDAC
Alexandria VA 22304-6145

Eglin AFB Offices:

WL/CA-N	1
WL/MNPM (Scientific & Tech Info Facility)	1
WL/MNS	1
WL/MNSA	5

WL/FIVCS 2
Attn: S. Strickland and M. Hughes
139 Barnes Drive, Suite 2
Tyndal AFB FL 32403-5323

WL/MLBC 2
Attn: K. Bowman and J. Mistretta
Wright Patterson AFB OH 45433-5000

DNA/SPSD 2
Attn: M. Giltrud and E. Wolfe
6801 Telegraph Road
Alexandria VA 22310-3398

ARPA/DSO 1
Attn: Dr. B. Wilcox
3701 N. Fairfax Drive
Arlington VA 22203-1714

AFOSR/NA 1
ATTN: Lt Col M. Lewis
110 Duncan Avenue, Suite B-115
Bolling AFB, DC 20332-0001

University of Florida 5
GERC
P O Box 1918
Eglin AFB FL 32542-0918

Dept. of Civil Engineering 1
Attn: Dr. J. Tedesco
Auburn Universtiy
Auburn AL 36849

Dept. of Civil Engineering 1
Attn: Dr. R. Sierakowski
470 Hitchcock Hall
2070 Neil Avenue
Columbus OH 43210-1275

USAE Wateways Experiment Station 1
CEWES-SD-R
Attn: S. Shore
3909 Halls Ferry Road
Vicksburg MS 39180-6199